MULTI-OBJECTIVE OPTIMIZATION OF A STEALTH UNMANNED COMBAT AERIAL VEHICLE

A Final Year Project Report

Presented to

SCHOOL OF MECHANICAL & MANUFACTURING ENGINEERING

Department of Mechanical Engineering

NUST

ISLAMABAD, PAKISTAN

In Partial Fulfillment of the
Requirements for the Degree of
Bachelors of Mechanical Engineering

---

by

Ammar Akram

Muhammad Fahad Zahid

Muhammad Ahsan Aziz

2019

EXAMINATION COMMITTEE

We hereby recommend that the final year project report prepared under our supervision by:

AMMAR AKRAM	00000126843
MUHAMMAD FAHAD ZAHID	00000129526
MUHAMMAD AHSAN AZIZ	00000127521

Titled: "**Multi-Objective Optimization of a Stealth Unmanned Combat Aerial Vehicle**" be accepted in partial fulfillment of the requirements for the award of **Mechanical Engineering** degree with grade ___

Supervisor: Dr. Emad Uddin, HoD (Assistant Professor)	Dated:
Committee Member: Dr. Ali Zaidi (Assistant Professor)	Dated:
Committee Member: Dr. Zaib Ali (Assistant Professor)	Dated:

_____ _____

(Head of Department) (Date)

COUNTERSIGNED

Dated: _____ _____

(Dean / Principal)

ABSTRACT

For Unmanned Combat Aerial Vehicles (UCAVs) operating during wartime, the mission objective is dependent on the **survivability** of the UCAV, which depends on two things:

1. Its ability to evade detection by enemy radars and scanners (Stealth)
2. Its ability to evade enemy fire when detected and fired upon. (Maneuverability).

This project entails the optimization of an Unmanned Combat Aerial Vehicle with **maximized survivability** to be used in conceptual phase of Aircraft Design. This shall be accomplished by means of a Multi-Objective Optimization, employing the Genetic Algorithm, with the objective functions being the Radar Cross Section (RCS) – which is to be minimized, and the Lift-to-Drag Ratio which signifies the Aerodynamic performance – which is to be maximized. Genetic Algorithm for Multi-Objective Optimization from MATLAB Optimization Toolbox is used. To minimize computational expense in the conceptual design phase, low fidelity methods for Lift to Drag Ratio and RCS calculations are used; Vortex Lattice Method (VLM) and Physical Optics (PO), respectively.

ACKNOWLEDGMENTS

We are all greatly indebted to Allah Almighty, who blessed us with the education and intellect to carry out this project. We would also like to acknowledge, in addition to our parents, all the teachers who taught us and inculcated within us the aspiration to serve humanity.

In particular, we would like to acknowledge the invaluable assistance provided by our supervisors, Dr. Adnan Maqsood and Dr. Emad-ud-din during the course of this project.

Moreover, we are thankful to Dr. David C. Jenn, of Naval Postgraduate School, CA, USA, Dr. Imran Mir of RCMS, NUST, Syed Hamza and Zia-ud-Din Taj of Pakistan Aeronautical Complex, Kamra for their assistance in the successful completion of this project.

Akram, Ammar; Zahid, Muhamad F.; Aziz, Muhammad A.; Multi-Objective Optimization of a Stealth Unmanned Combat Aerial Vehicle

ORIGINALITY REPORT

17%	9%	9%	14%
SIMILARITY INDEX	INTERNET SOURCES	PUBLICATIONS	STUDENT PAPERS

PRIMARY SOURCES

1	aerodynamics.aeromech.usyd.edu.au Internet Source	3%
2	Submitted to Cranfield University Student Paper	1%
3	en.wikipedia.org Internet Source	1%
4	Submitted to North West University Student Paper	1%
5	Submitted to Universidad Carlos III de Madrid Student Paper	1%
6	R. Mukesh, K. Lingadurai, U. Selvakumar. "Airfoil shape optimization using non-traditional optimization technique and its validation", Journal of King Saud University - Engineering Sciences, 2014 Publication	1%
7	Arora, Rajesh. "Guided Random Search	

	Methods", Optimization, 2015. Publication	1%
8	Submitted to Engineers Australia Student Paper	1%
9	David C. Jenn. "Radar Cross-Section", Wiley, 2005 Publication	<1%
10	Jacques Periaux, Felipe Gonzalez, Dong Seop Chris Lee. "Evolutionary Optimization and Game Strategies for Advanced Multi-Disciplinary Design", Springer Science and Business Media LLC, 2015 Publication	<1%
11	Submitted to University of Sheffield Student Paper	<1%
12	etd.auburn.edu Internet Source	<1%
13	Submitted to University of Liverpool Student Paper	<1%
14	www.leobaumann.de Internet Source	<1%
15	Submitted to University of Technology, Sydney Student Paper	<1%
16	Submitted to Technische Universiteit Delft Student Paper	<1%

17	Submitted to Middle East Technical University Student Paper	<1%
18	dspace.lib.cranfield.ac.uk Internet Source	<1%
19	docplayer.net Internet Source	<1%
20	Submitted to University of Hertfordshire Student Paper	<1%
21	Submitted to Korea Aerospace University Graduate School Student Paper	<1%
22	www.iare.ac.in Internet Source	<1%
23	Submitted to University of Surrey Student Paper	<1%
24	www.scribd.com Internet Source	<1%
25	Submitted to University of Salford Student Paper	<1%
26	Submitted to Queen Mary and Westfield College Student Paper	<1%
27	Thomas Rylander, Jian-Ming Jin. "Perfectly matched layer for the time domain finite	<1%

element method", Journal of Computational Physics, 2004
Publication

---

28 Hosein Taghdisian, Mahmoud Reza Pishvaie, Fatola Farhadi. "Multi-objective optimization approach for green design of methanol plant based on CO2-efficeincy indicator", Journal of Cleaner Production, 2015 — <1%
Publication

---

29 Submitted to Institute of Graduate Studies, UiTM — <1%
Student Paper

---

30 R. Mukesh. "Aerodynamic optimization using proficient optimization algorithms", 2012 International Conference on Computing Communication and Applications, 02/2012 — <1%
Publication

---

31 radiocomp.ru — <1%
Internet Source

---

32 Kulfan, Brenda. "Recent Extensions and Applications of the "CST" Universal Parametric Geometry Representation Method", 7th AIAA ATIO Conf 2nd CEIAT Int l Conf on Innov & Integr in Aero Sciences 17th LTA Systems Tech Conf followed by 2nd TEOS Forum, 2007. — <1%
Publication

R.T. Marler, J.S. Arora. "Survey of multi-

33	objective optimization methods for engineering", Structural and Multidisciplinary Optimization, 2004 Publication	<1%
34	Submitted to University of Glamorgan Student Paper	<1%
35	Encyclopedia of Earth Sciences Series, 2014. Publication	<1%
36	uknowledge.uky.edu Internet Source	<1%
37	Tadashi Sato. "Calculation of three-dimensional static magnetic field by equivalent current of magnetization vector and its applications", Electrical Engineering in Japan, 03/1980 Publication	<1%
38	P. Ratanadecho, K. Aoki, M. Akahori. "A numerical and experimental investigation of the modeling of microwave heating for liquid layers using a rectangular wave guide (effects of natural convection and dielectric properties)", Applied Mathematical Modelling, 2002 Publication	<1%
39	Submitted to City University Student Paper	<1%
40	www.jevylee.com	

	Internet Source	<1%
41	Xiaohui Guan. "Supersonic Wing–Body Two-Level Wave Drag Optimization Using Extended Far-Field Composite-Element Methodology", AIAA Journal, 2014 Publication	<1%
42	Harry R. Anderson. "Fixed Broadband Wireless System Design", Wiley, 2003 Publication	<1%
43	Long, D. Leann, John S. Preisser, Amy H. Herring, and Carol E. Golin. "A marginalized zero-inflated Poisson regression model with overall exposure effects", Statistics in Medicine, 2014. Publication	<1%
44	Submitted to University of Bristol Student Paper	<1%
45	vdocuments.mx Internet Source	<1%
46	Submitted to Glyndwr University Student Paper	<1%
47	Adaptation Learning and Optimization, 2010. Publication	<1%
48	ethesis.nitrkl.ac.in Internet Source	

		<1%
49	etd.lib.fsu.edu Internet Source	<1%
50	Submitted to Higher Education Commission Pakistan Student Paper	<1%
51	www2.elo.utfsm.cl Internet Source	<1%
52	P. Ratanadecho. "A NUMERICAL AND EXPERIMENTAL STUDY OF MICROWAVE DRYING USING A RECTANGULAR WAVE GUIDE", Drying Technology, 9/30/2001 Publication	<1%
53	Submitted to Loughborough University Student Paper	<1%
54	Submitted to Coventry University Student Paper	<1%
55	Submitted to University of Wales Swansea Student Paper	<1%
56	mafiadoc.com Internet Source	<1%
57	Kulfan, B. M.. "Recent extensions and applications of the ‘CST’ universal parametric geometry representation method", The	<1%

Aeronautical Journal, 2010.
Publication

---

58 Jiwei Tang, Yu Hu, Bifeng Song, Hui Yang. "Unsteady Aerodynamic Optimization of Airfoil for Cycloidal Propellers Based on Surrogate Model", Journal of Aircraft, 2017 — <1%
Publication

---

59 Kobayashi, Michikazu, and Muneto Nitta. "Vortex Polygons and Their Stabilities in Bose-Einstein Condensates and Field Theory", Journal of Low Temperature Physics, 2014. — <1%
Publication

---

60 www.asdl.gatech.edu — <1%
Internet Source

---

61 E. I. Veliev, Kamil Karacuha, Ertucrul Karaguha. "Scattering of a Cylindrical Wave from an Impedance Strip by Using the Method of Fractional Derivatives", 2018 XXIIIrd International Seminar/Workshop on Direct and Inverse Problems of Electromagnetic and Acoustic Wave Theory (DIPED), 2018 — <1%
Publication

---

62 Submitted to Emirates Aviation College, Aerospace & Academic Studies — <1%
Student Paper

---

63 Sadraey, . "Wing Design", Aircraft Design A Systems Engineering Approach, 2012. — <1%

	Publication	
64	Submitted to Embry Riddle Aeronautical University Student Paper	<1%
65	www.igi-global.com Internet Source	<1%
66	Submitted to Koc University Student Paper	<1%
67	elektroarsenal.net Internet Source	<1%
68	Submitted to International Centre for Integrated Mountain Development (ICIMOD) Student Paper	<1%
69	Submitted to Sheffield Hallam University Student Paper	<1%
70	Zhang, Jiahui, Jason Waggel, Dave Weber, and Tony Pollice. "Numerical and Experimental Analysis for Air Circulation and Cooling Performance in a Cell Cabinet", ASME 2007 InterPACK Conference Volume 1, 2007. Publication	<1%
71	Cary, Jason, and Gil Crouse. "Preliminary Design Optimization of an Amphibious Aircraft", 50th AIAA Aerospace Sciences Meeting including the New Horizons Forum and Aerospace Exposition, 2012.	<1%

Publication

72	meeng.technion.ac.il Internet Source	<1%
73	D.J. Nelson. "A coupled thermal magnetic model for high frequency transformers. I. Model formulation and material properties", IEEE Transactions on Components Hybrids and Manufacturing Technology, 1992 Publication	<1%
74	archive.org Internet Source	<1%
75	Emidio Marchetti, Rui Du, Ben Willetts, Fatemeh Norouzian et al. "Radar cross-section of pedestrians in the low-THz band", IET Radar, Sonar & Navigation, 2018 Publication	<1%
76	Submitted to Monash University Student Paper	<1%
77	Mamun, Abdullah, Ziad Shawwash, Alaa Abdalla, Jian Li, and Thomas Siu. "Application of a goal programming algorithm to incorporate environmental requirements in a multi-objective Columbia River Treaty Reservoir optimization model", Canadian Water Resources Journal / Revue canadienne des ressources hydriques, 2015. Publication	<1%

78	Cristhian P. Almeida-Rivera, Johan Grievink. "Process Design Approach for Reactive Distillation Based on Economics, Exergy, and Responsiveness Optimization", Industrial & Engineering Chemistry Research, 2008 Publication	<1%
79	Submitted to American Public University System Student Paper	<1%
80	Kulfan, Brenda. "A Universal Parametric Geometry Representation Method - "CST"", 45th AIAA Aerospace Sciences Meeting and Exhibit, 2007. Publication	<1%
81	Lane, Kevin, and David Marshall. "Inverse Airfoil Design Utilizing CST Parameterization", 48th AIAA Aerospace Sciences Meeting Including the New Horizons Forum and Aerospace Exposition, 2010. Publication	<1%

Exclude quotes	On	Exclude matches	Off
Exclude bibliography	On		

TABLE OF CONTENTS

LIST OF FIGURES

LIST OF TABLES

ABBREVIATIONS

AVL	Athena Vortex Lattice
CA	California
CFD	Computational fluid Dynamics
CST	Class Shape Transformation
ECM	Electronic Counter Measures
FDM	Finite Difference Method
FEM	Finite Element Method
GA	Genetic Algorithm
MoM	Method of Moments
NUST	National University of Sciences and Technology
PO	Physical Optics
RCMS	Research Center for Modelling and Simulation
RCS	Radar Cross Section
TE	Transverse Electric
TM	Transverse Magnetic
TPM	Technical performance Measures
UCAV	Unmanned Combat Aerial Vehicle
VLM	Vortex Lattice Method

NOMENCLATURE

A	Magnetic Vector Potential (Wb/m)
B	Magnetic Flux Density (Wb/m^2)
$C_{D\ TO}$	Take-off Drag coefficient
C_{Dmin}	Minimum drag coefficient
C_{dmin}	Minimum Drag coefficient
$C_{L\ TO}$	Take-off Lift coefficient
$C_L/C_{d\ max}$	Maximum Lift-drag ratio
C_{lalpha}	Lift-Curve Slope
C_{Lc}	Cruise Lift Coefficient
C_{Lc}	Aircraft Cruise Lift Coefficient
C_{LCw}	Wing Cruise Lift Coefficient
C_{Lcw}	Wing Cruise Lift Coefficient
C_{Li}	Wing Ideal Lift Coefficient
C_{Lmax}	Max Lift Coefficient
C_{Lmax}	Aircraft Max Lift Coefficient
C_{lmax}	Maximum Lift Coefficient
C_{LmaxG}	Aircraft Gross Lift Coefficient
$C_{L\alpha max}$	C_L corresponding to maximum allowable α
$C_{m'inc}$	Pitching moment coefficient corresponding to cruise
$C_{m'max}$	Pitching moment coefficient corresponding to maximum allowable α
C_{mo}	Pitching moment coefficient corresponding to $\alpha=0°$

D	Electric Flux Density (C/m^2)
E	Electric field Intensity (V/m)
F	Electric Vector Potential (C/m)
g	Gravitational acceleration (m/s^2)
H	Magnetic field intensity (A/m)
h_{sc}	Service Ceiling (m)
J	Volume Current Density (A/m^2)
J_s	Surface Current Density (A/m)
k	Induced drag coefficient
M	Magnetic Current Density (V/m^2)
MTOW	Maximum Take-off Weight (N)
n	Load factor
P_s	Specific energy level at condition (m/s)
q	Dynamic pressure at condition (N/m^2)
R	Target Range (m)
ROC	Rate of Climb (m/s)
S	Wing reference area (m^2)
S_{TO}	Take-off Run (m)
T	Thrust (N)
V_c	Cruise speed (m/s)
V_{LOF}	Lift-off speed (m/s)
V_{MAX}	Maximum Speed (m/s)

V_{STALL}	Stall Speed (m/s)
$V_{SUSTURN}$	Sustained Turn Speed (m/s)
V_{TO}	Take-off Speed (m/s)
V_v	Rate of climb (m/s)
W	Weight (N)
W_{ave}	Average Aircraft Weight (N)
W_{TO}	Take-off Weight (N)
$\alpha_{CL/Cd\ max}$	AOA corresponding to $(C_L/C_d)_{max}$
α_{Stall}	Stall angle (deg)
ε	Permittivity (F/m)
θ_{MAX}	Bank angle at maximum Load Factor (deg)
μ	Ground friction coefficient
μ	Permeability (H/m)
ρ	Air density (kg/m^3)
ρ_v	Volumetric charge density (C/m^3)
σ	Radar Cross Section (m^2)
ω	Angular Frequency (rad/s)

CHAPTER 1: INTRODUCTION

Close Air Support in Modern Warfare

With the progression of technology, modern warfare is evolving to be less reliant on humans, directly engaged in the battlefield and more on robots and unmanned systems to minimize human casualties and increase effectiveness. For infantry attacks, Close Air Support (CAS) is crucial, which has conventionally been accomplished by means of aircraft such as the A-10 Warthog. The nature of the mission requires flying at dangerously low speeds and altitudes and extremely high strafing precision, which makes the job of the pilot extremely difficult and not to mention risky. Moreover, such aircraft are sluggish and vulnerable to enemy fire, and can attack a limited region at a time before returning to base for re-armament.

Survivability of a UCAV

For UCAVs operating in military engagement zones, the mission objective is dependent on the survivability of the UCAV, which depends on two things:

1. Its ability to evade detection by enemy radars and scanners (Stealth)
2. Its ability to evade enemy fire when detected and fired upon. (Maneuverability).

Project Objective

Therefore, it is the need of the hour for Pakistan to develop a Close Air Support Unmanned Combat Aerial Vehicle with **maximized survivability**, capable of being employed effectively in swarms, which is the objective of this project.

To accomplish this objective, the development of the UCAV is going to be focused on coming up with an optimized design that results from:

A. Minimizing the Radar Cross Section (RCS)
B. Maximizing the Aerodynamic performance

Both these objectives depend on airfoil and planform profiles of wing (Material is ignored here). In this work, only planform shape is optimized.

CHAPTER 2: LITERATURE REVIEW

The Aircraft Design Process

In cognizance of the fact that this is an aircraft design project, the first step in the order of affairs was to acquaint ourselves with the design process that is the norm in the aerospace industry. For this, various approaches were studied, out of them, the most suitable one for us was evidently the Systems Engineering approach to aircraft design. This approach constitutes of treating each aircraft system as a sub-set of the aircraft to be designed and integrates these designs as the process progresses. It consists of the following phases:

1. Ascertaining of operational requirements
2. Mission synthesis
3. Drafting of Technical Performance Measures (TPMs)
4. Conceptual design
5. Preliminary design
    i. Weight sizing
    ii. Constraint analysis
6. Detailed design
    i. Wing design
    ii. Fuselage design
    iii. Tail design
    iv. Propulsion system design
    v. Control surface design
7. Integration of components
8. Balancing
9. Aircraft Stability and Performance analysis
10. Prototype development
11. Static Testing
12. Flight Testing
13. Commissioning

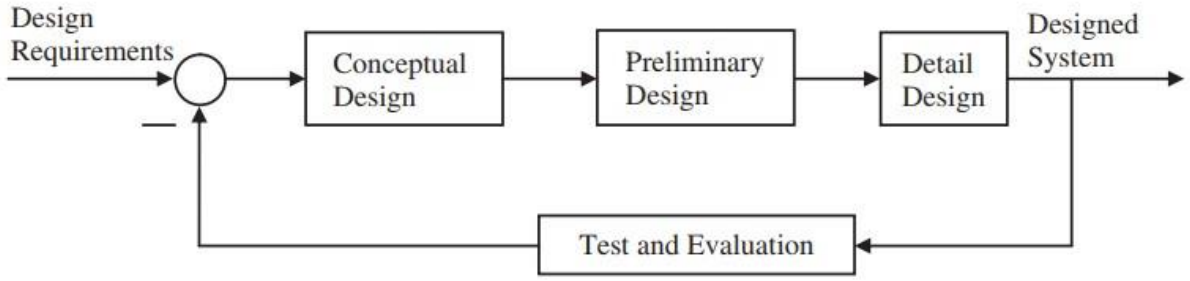

Figure 1: The systems Engineering Approach to Aircraft Design *(1)*

Baseline Selection

In the Concept Design phase of the design process, one of the approaches is to take into consideration existing, proven designs that come close to TPMs. These aircraft are termed as baselines and are subsequently modified so as to fulfill the TPMs, this is especially true for aircraft designed as a result of extensive research such as Stealth aircraft, so as to build upon the results of that research rather than reinventing the wheel.

For the selection of suitable baselines, it is imperative for a comparison to be drawn, the type of comparison is dependent on the priorities of the designer and the nature of the project. For purposes of our project, the priorities are to have a minimal RCS, and maximum Aerodynamic performance. For evaluating and subsequently drawing up a comparison between the baselines, it is imperative for an analysis to be conducted, this analysis can be computational or a physical one.

Aerodynamic Analysis

For evaluation of the aerodynamic characteristics of the baseline aircraft, owing to the classified status of performance data, a Computational Fluid Dynamics (CFD) simulation is to be conducted. Available options for the simulation include:

Table 1: Comparison of CFD Methods

		Advantages	***Disadvantages***
High-Fidelity Methods	*Reynolds-Averaged-Navier Stokes* *Large-Eddy Simulation* *Detached-Eddy Simulation*	High accuracy	Computationally intensive

Low-Fidelity Methods	*Panel Methods*	Quick, suitable for inviscid flow	Not suitable for viscous flow analysis, boundary layers and flow separation.

Vortex Lattice Method

The Vortex Lattice Method (2) models an aircraft's lifting surfaces as an infinitely thin sheet of discrete vortices for the purposes of computing aerodynamic characteristics such as lift and induced drag. The influence of the thickness and viscosity is neglected.

For the course of this project, has been used to draw a relative comparison between the aerodynamic characteristics of the competing baselines. The justification for its selection, in spite of the inviscid approximation, is the low operational speed of the aircraft which is around Mach 0.08, the flow at which can be approximated with inviscid simplification at a fairly low penalty with regards to accuracy. The feature of easy coupling with MATLAB, is an added plus, along with quick computations make it ideal for the task of computing relative aerodynamic performances of the potential baseline aircraft.

The power of VLM lies in its ability to approximate flows around objects ranging from as simple as a Hershey-bar wing to a full-fledged Trapezoidal wing, complete with rivets, NACA ducts, pitot tubes etc. It is widely used in the aircraft industry in the initial design stages to quickly evaluate aerodynamic performances of different concepts.

Upon simulation of the flow field, the force distribution, consequently the pressure distribution, can be extracted. From this data, one can get the aerodynamic coefficients, which signify the aerodynamic efficiency, maneuverability, stability and performance of the aircraft. The pressure distribution can also serve as important input for the structural designers to get an approximation of the stresses on the wing.

The VLM is the extension of Prandtl lifting line theory, wherein the wing of an aircraft is modeled as an infinite number of Horseshoe vortices, in the form of lattices. The number of which is a function of accuracy.

This method neglects all viscous effects. Turbulence, dissipation and boundary layers are not resolved at all. However, lift induced drag can be assessed and, taking special care, some stall phenomena can be modelled.

The following assumptions (2) are made regarding the problem in the vortex lattice method:

1. The flow is not compressible, we have assumed zero viscosity and irrotational flow. However, if we use 3D Prandtl Glauert transformation in this method then we can address the issue of small localized-disturbance low subsonic compressible flows. The effect of thickness on aerodynamic forces has been neglected.
2. We have applied small angle approximation on the slip-side angle and angle of attack.

Flow on a Generic 3-D Wing

We can use VLM to obtain 3D solution for flow on a generic wing. Panels consist of horse-shoe vortices. Bound vortex is positioned at quarter-chord position with two lines of trailing vortices at each end. We can model variations in lift along the span as well as along the chord.

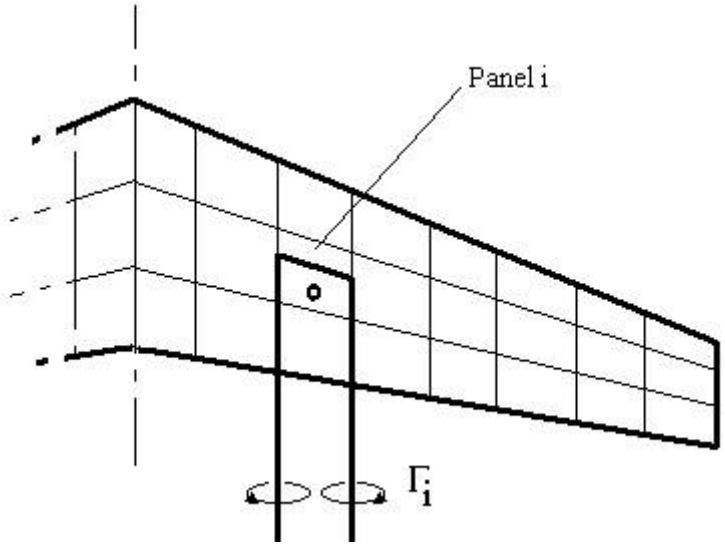

Figure 2: Vortex Lattice on a generic wing *(3)*

The required strength of the bound vortex on each panel will need to be calculated by applying a surface flow boundary condition. The equation used is the usual condition of zero flow normal to the surface. For each panel the condition is applied at the 3/4 chord position along the center line of the panel. The normal velocity is made up of a freestream component and an induced flow component. This induced component is a function of strengths of all vortex panels on the wing. Thus, for each panel an equation can be set up which is a linear combination of the effects of the strengths of all panels. A matrix of influence coefficients is created which is multiplied by the vortex strengths and equal to a right-hand side vector of freestream effects.

$$V_n = 0 = V_\infty sin(\theta) + w_i$$
$$w_i = \Sigma_{j=1}^{N} A_{ij}\Gamma_j$$
$$\Sigma_{j=1}^{N} A_{ij}\Gamma_j = -V_\infty sin(\theta)$$

Influence coefficient $\mathbf{A}_{ij}$ represents induced flow over the panel owing to panel j's vortex. Assuming all panels to be planar, influence coefficient is calculated by application of the Biot-Savart law along the three vortex line components.

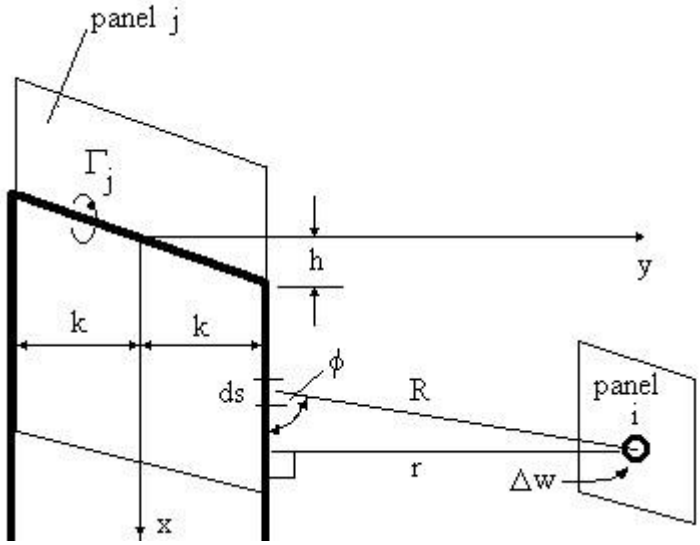

Figure 3: Panel parameters *(3)*

Integration results in the following formula:

$$\Delta w = \frac{1}{4\pi}\frac{sin(\phi)}{r^2}\Gamma_j.ds$$
$$w_{ij} = \int \frac{1}{4\pi}\frac{sin(\phi)}{r^2}.ds.\Gamma_j = A_{ij}\Gamma_j$$

Solving further

$$A_ij = \frac{1}{4\pi}(A_{bound} + A_{left} + A_{right})$$

where

$$A_{bound} = \frac{1}{(x+h)(y-k)-(x-h)(y+k)} \cdot \left(\frac{2h(x+h)+2k(y+k)}{R_1} - \frac{2h(x-h)+2k(y-k)}{R_2} \right)$$

$$A_{left} = -\frac{1}{(y+k)} \cdot \left(1 + \frac{x+h}{R_1} \right)$$

$$A_{right} = \frac{1}{(y-k)} \cdot \left(1 + \frac{x-h}{R_2} \right)$$

$$R_1 = \sqrt{(x+h)^2 + (y+k)^2)}$$

$$R_2 = \sqrt{(x-h)^2 + (y-k)^2)}$$

The RHS terms for the boundary condition equations depend on freestream velocity, angle of attack and slope of the panels owing to the effect of camber.

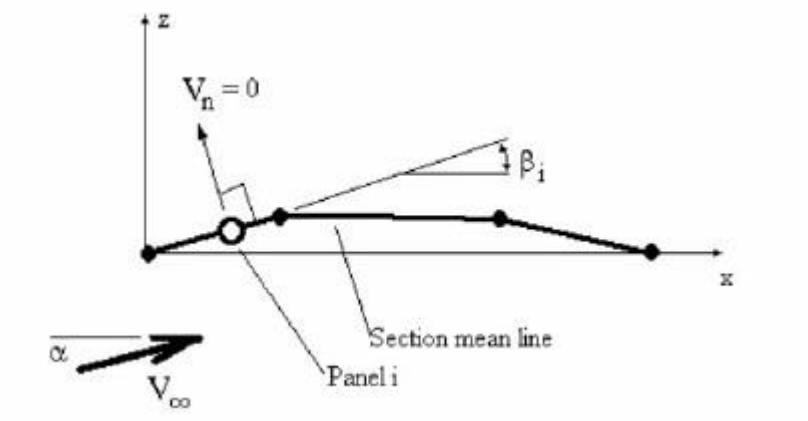

$$sin(\theta) = sin(\alpha - \beta_i) \approx \alpha - \beta_i \approx \alpha - \left(\frac{dz}{dx} \right)_i$$

Figure 4: Effect of Camber *(3)*

Assuming all angles to be small. The solution for vortex line strength is found by solving the matrix of equations.

The lift coefficient for the wing at a given angle of attack will be obtained by integrating the panel lift distribution. The lift on a particular panel can be found using the Kutta Law.

$$L_i = \rho V_\infty \Gamma_i 2k$$

Which is the lift of panel **i**.

Therefore, lift of wing is the sum of all panel lifts,

$$L = \Sigma_{i=1}^{N} L_i$$

The downwash fluid velocity induced on the panel can be obtained after finding the strength of wing loading. As a result of this downwash flowing fluid, the direction of lift vector is rotated. The localized lift vectors are rotated in the backward direction and therefore produce a lift induced drag. Integrating the panel lift coefficient components, acting parallel to the free stream flowing across span. This the induced drag coefficient can be found.

$$D_i = \rho V_\infty \Gamma_i sin(\alpha_i)$$

Which represents drag from panel **i**. Hence, the lift-induced-drag of wing can be represented by the formula:

$$D_{induced} = \Sigma_{i=1}^{N} D_i$$

Induced flow angle ($\boldsymbol{\alpha_i}$) shows rotation of lift vector in the reverse direction and therefore it should be obtained from velocities induced on bound vortices of the panel by other panels and induced by the freestream.

Pitching moment about the leading edge of the wing root can be obtained by summing the product of panel lift and the moment arm extending along the x axis from the leading edge to the mid of the bound vortex of the panel.

Radar Cross-Section Engineering

Radar Countermeasures

Consider a combat scenario where it is required to attack a high-profile ground target surrounded by a network of radars. The circles in figure 5 represent maximum detection ranges of individual radars. There are two methods of deceiving radars in such a situation (4):

1) Low Observability or "stealth". In this approach, the radar detectability of a target is reduced. This is accomplished by reducing target's radar cross section. However, radar range (R) and radar cross section σ are related as $\sigma \sim R^4$, which means a significant reduction in RCS is required to achieve a small reduction in radar range.
2) Electronic Countermeasures (ECM). Here, the range is suppressed by inducing noise through *chaff* (metal pieces whose return is so large that it suppresses target's presence) or through *jamming (Figure 6).* These are passive and active ECM methods, respectively. Modern radars have a defense mechanism against ECM so various combinations of stealth and ECM are used.

As a final note, radars can be defeated entirely by stealth techniques. However, the cost may be very high along with performance, manufacturing and maintenance constraints, which is why the two techniques are employed simultaneously.

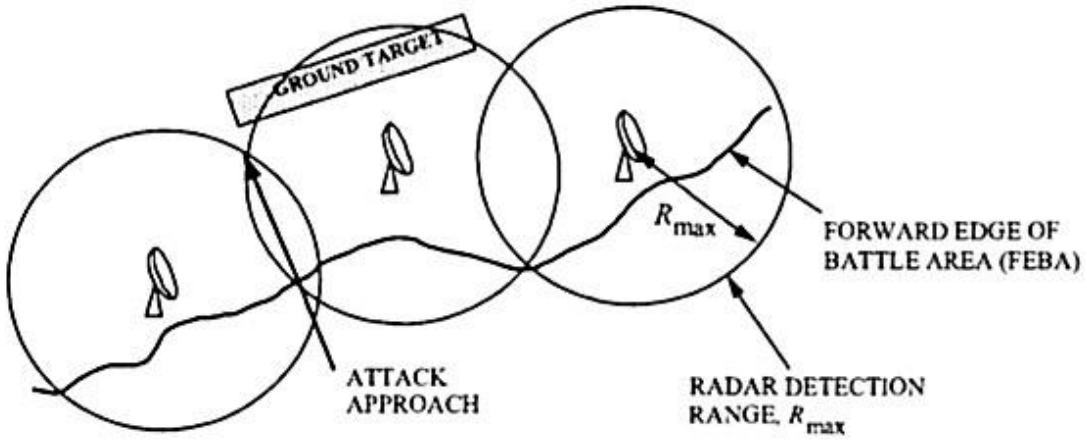

Figure 5: A network of radars arranged to provide continuous coverage of a ground target *(4)*

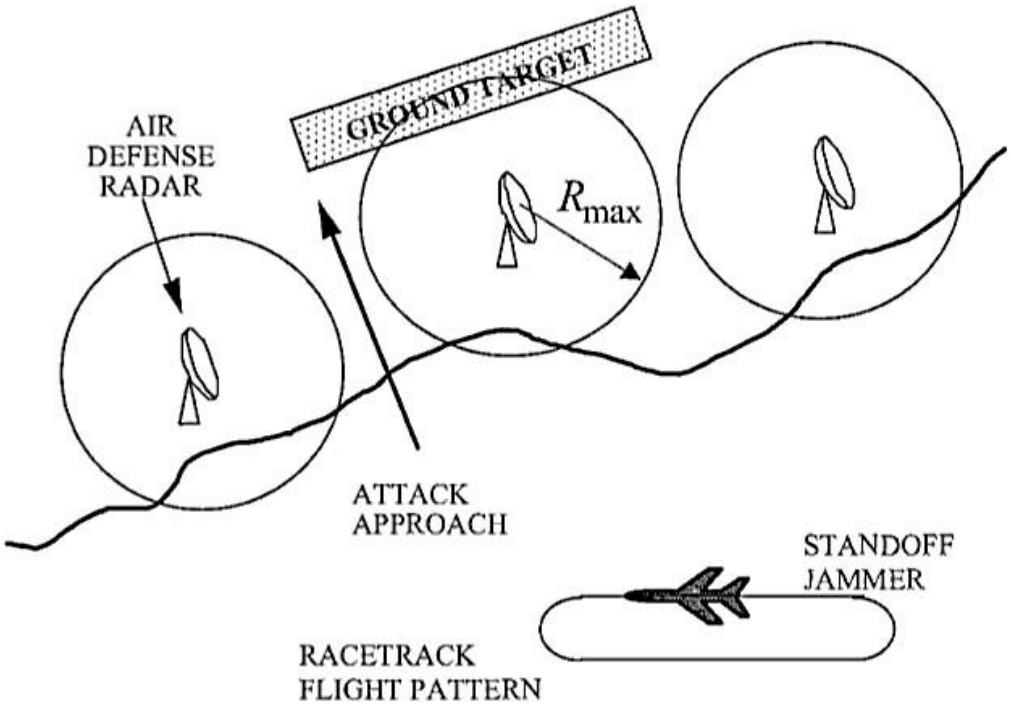

Figure 6: Standoff jammer operating against a network of radars *(4)*

Radar Cross Section (RCS)

RCS (σ) or echo area characterizes the radar detectability of a target. It is the of echo signal returned to the radar by the target. Formally, it is defined as, "the area intercepting the amount of power that, when scattered isotropically, produces at the receiver a density that is equal to the density scattered by the actual target" (5). Mathematically (4),

$$\sigma \equiv \frac{Power\ relected\ to\ reciever\ per\ uni\ solid\ angle}{Incident\ power\ density\ /_{4\pi}}$$

$$\sigma = \lim_{R\to\infty} 4\pi R^2 \frac{\left|\overrightarrow{E_s}\right|^2}{\left|\overrightarrow{E_i}\right|^2} = \lim_{R\to\infty} 4\pi R^2 \frac{\left|\overrightarrow{W_s}\right|^2}{\left|\overrightarrow{W_i}\right|^2}$$

Where,

W_s, W_i = Scattered, Incident field power density

E_s,E_i = Scattered, Incident Electric field

R = Target Range

$$\sigma, dBsm = 10\log(\sigma, m)$$

The commonly used unit of RCS is decibels square meters

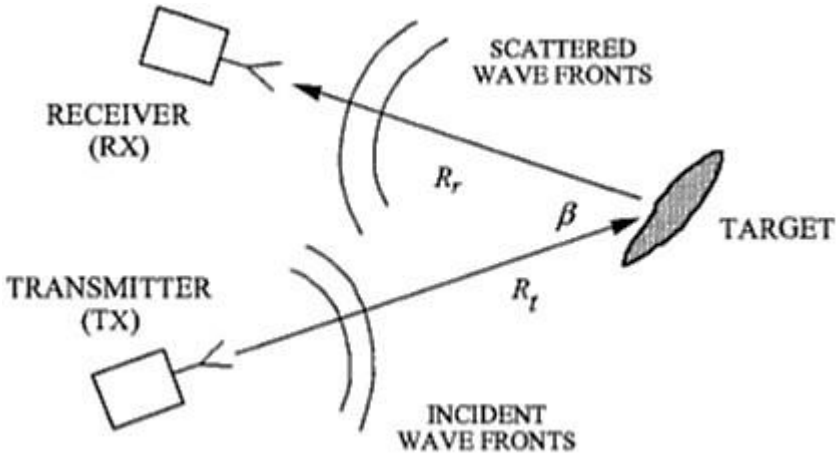

Figure 7: Bistatic Radar *(4)*

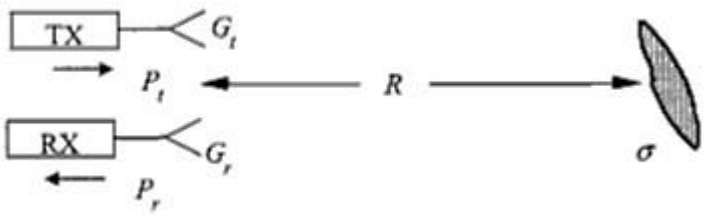

Figure 8: Monostatic Radar *(4)*

When radar transmitter and receiver are located at the same location, the radar is called *monostatic* radar. Generally, they are at different locations and the radar is called *bistatic* (shown in figure 7). If the two antennas are slightly separated, such a radar is called *quasi monstatic* (as illustrated in Figure 8). A stealth platform designed for monostatic radars is not stealthy for bistatic radars. This work focuses on monostatic case only. Typical values of RCS are shown in figure 8.

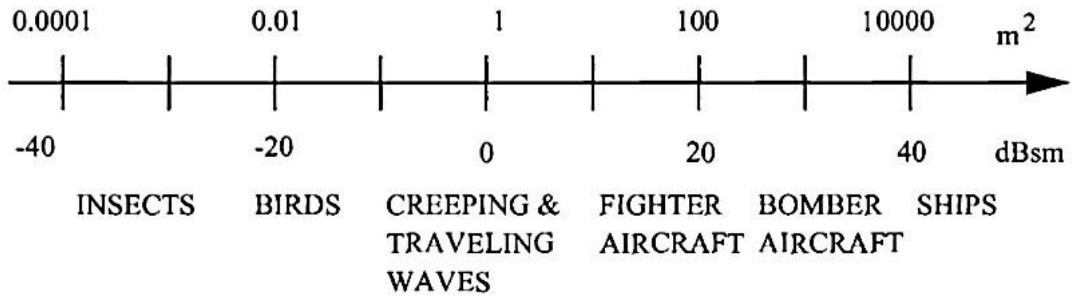

Figure 9:Typical values of RCS for some natural and man-made objects *(4)*

Following information about the target is available from radar echo:

1) Range
2) Velocity
3) Direction
4) Size
5) Shape
6) Propellers and turbines, from targets moving components

Factors on which RCS depends

1) Radar's frequency and bandwidth
2) Radar's transmit antenna polarization
3) Radar's receive antenna polarization

4) Shape of the Target
5) Target Aspect (its orientation relative to the radar)
6) Materials of which target is composed
7) Radar/Target geometry

Polarization

Polarization of a radiated wave is defined as "that property of an electromagnetic wave describing the time-varying direction and relative magnitude of the electric-field vector; specifically, the figure traced as a function of time by the extremity of the vector at a fixed location in space, and the sense in which it is traced, as observed along the direction of propagation" (4). As a rule of thumb, "Polarization is the curve traced by the end point of the arrow (vector) representing the instantaneous electric field" (4). Polarization is classified as linear and circular (as illustrated in figure 10)

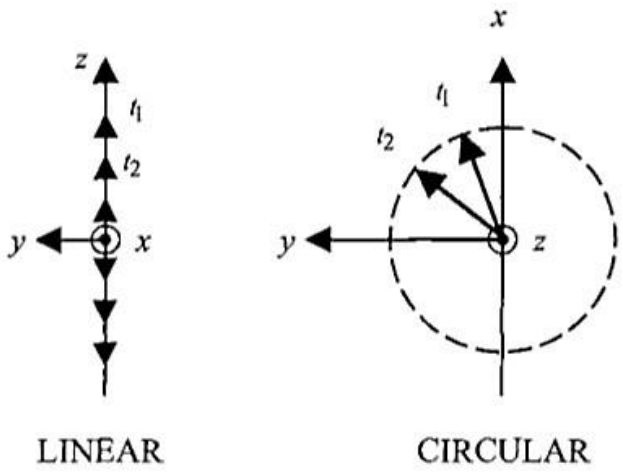

Figure 10: Illustration of linear and circular polarizations *(4)*

Linear polarization is further classified as Transverse Electric (TE) and Transverse Magnetic (TM). If z-axis is used as reference, TE_z refers to electromagnetic wave with time varying electric field along the plane transverse to the z-axis

Frequency Bands

Since RCS depends on frequency, it is worthwhile to discuss the frequency bands commonly used in modern radars. Table 2 shows frequency bands with respective frequency ranges.

Table 2: Radar Frequency Bands

Band designation	**Frequency Range**
HF	3-30 MHz
VHF	30-300 MHz
UHF	300-1000 MHz
L	1-2 GHz
S	2-4 GHz
C	4-8 GHz
X	8-12 GHz
Ku	12-18 GHz
K	18-27 GHz
Ka	27-40 GHz
MM	40-300 GHz

Methods of Radar Cross Section Prediction

From the definition of RCS, it is evident that calculation of RCS requires computation of scattered electric field. A target when illuminated by radar waves essentially behaves as an antenna. A surface current is induced on it which is very difficult to determine. One can also use the Maxwell's equations (Table 2) for computation of scattered electric field. Reference 1 enlists the following methods for this purpose, the details of which can be found in advanced Electromagnetics texts.

a) Physical Optics (PO)
b) Microwave Optics
c) Method of Moments (MoM)
d) Finite Element Method (FEM)
e) Finite Difference Method (FDM)

Physical Optics (PO)

The scattered electromagnetic field is set up by induced surface current on the target body. This field can be determined by Radiation Integrals. The currents induced on the body are usually not known. Physical Optics method provides a very good guess for surface current by directly illuminating the target by the incident field. The current on the shadowed potions is set to zero (as shown in figure 11). If surface electric current density (Amperes/meter) is represented by J_s then physical optics theorem is stated mathematically as

$$\vec{J}_s \approx 2\hat{n} \times \vec{H}_i \text{ for illuminated portions}$$

$$\vec{J}_s \approx 0 \text{ for shadowed portions}$$

Where, $\vec{H}_i$ is the scattered magnetic field intensity at the surface and $\hat{n}$ is the local surface normal unit vector.

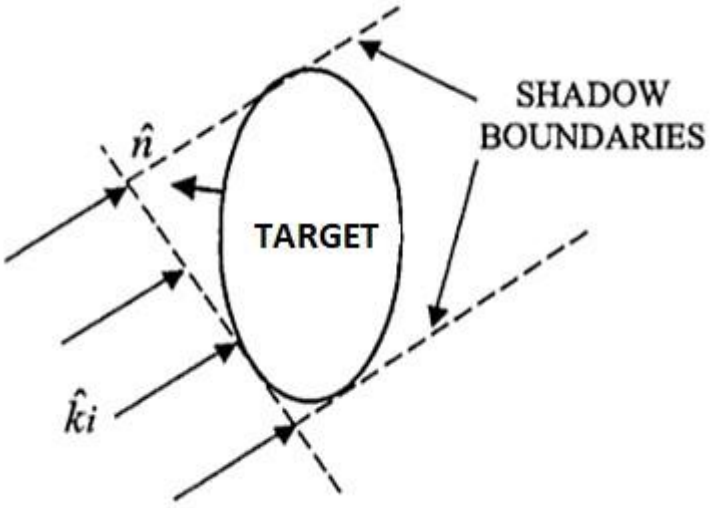

Figure 11: Illuminated and shadowed parts of a surface for application of the physical optics approximation *(4)*

The reader is advised to understand similar theorems (e.g. Uniqueness theorem, Image Theory, Duality Theorem and Equivalence Principle) from reference (4) and (5) before trying to understand physical optics theorem. The derivation of PO theorem can be seen in these references.

Calculation of Scattered Fields

Electromagnetic fields due to electric and magnetic currents can be computed directly from Maxwell's Equations (Table 3). A longer but mathematically convenient method is to use auxiliary potential functions. This is depicted in block diagram in figure 12 (6).

Table 3: Generalized form of Maxwell's Equations *(7)*

Differential Form	Integral Form
$\nabla . \boldsymbol{D} = \boldsymbol{\rho_v}$	$\oint \boldsymbol{D} . dS = \iiint \rho_v dv$
$\nabla . \boldsymbol{B} = \boldsymbol{0}$	$\oint \boldsymbol{B} . dS = 0$
$\nabla \times \boldsymbol{E} = -\frac{\partial \boldsymbol{B}}{\partial \boldsymbol{t}}$	$\oint \boldsymbol{E} . d\boldsymbol{l} = -\frac{\partial}{\partial t} \iint \boldsymbol{B} . d\boldsymbol{S}$
$\nabla \times \boldsymbol{H} = \boldsymbol{J} + \frac{\partial \boldsymbol{D}}{\partial \boldsymbol{t}}$	$\int \boldsymbol{H} . d\boldsymbol{l} = \iint \left(\boldsymbol{J} + \frac{\partial \boldsymbol{D}}{\partial t} \right) . d\boldsymbol{S}$

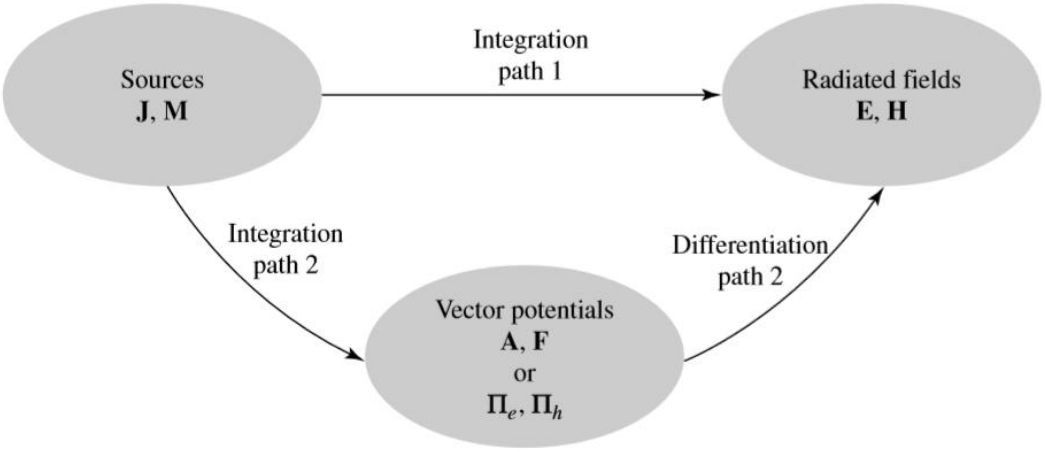

Figure 12: Block diagram for computing fields radiated by electric and magnetic sources *(6)*

Using path 2 along with physical optics and considering the coordinate system shown in figure 14, the radar cross section determination can be summarized as follows (6):

1. Specify **J** and **M**; here they are found using physical optics
2. Find **A** due to **J** using

$$\boldsymbol{A} = \frac{\mu}{4\pi} \iiint \boldsymbol{J} \frac{e^{-jkR}}{R} dv'$$

3. Find **F** due to **M** using

$$\boldsymbol{F} = \frac{\epsilon}{4\pi}\iiint \boldsymbol{M}\frac{e^{-jkR}}{R}dv'$$

Where, $k^2 = \omega^2\mu\epsilon\epsilon$

4. The total fields can then be determined by

$$\boldsymbol{E} = \boldsymbol{E_A} + \boldsymbol{E_F} = -j\omega\boldsymbol{A} - j\frac{1}{\omega\mu\epsilon}\nabla(\nabla.\boldsymbol{A}) - \frac{1}{\epsilon}\nabla\times\boldsymbol{F}$$

And

$$\boldsymbol{H} = \boldsymbol{H_A} + \boldsymbol{H_F} = -j\omega\boldsymbol{F} - j\frac{1}{\omega\mu\epsilon}\nabla(\nabla.\boldsymbol{F}) + \frac{1}{\mu}\nabla\times\boldsymbol{A}$$

5. Finally, RCS can be calculated using Physical Optics Theorem as stated above.

Limitations of Physical Optics Approximation (4)

1. PO is a high frequency approximation.
2. It gives the most accurate results in specular direction.
3. Diffraction, Multiple Reflections, Shadowing, Surface waves are not included.

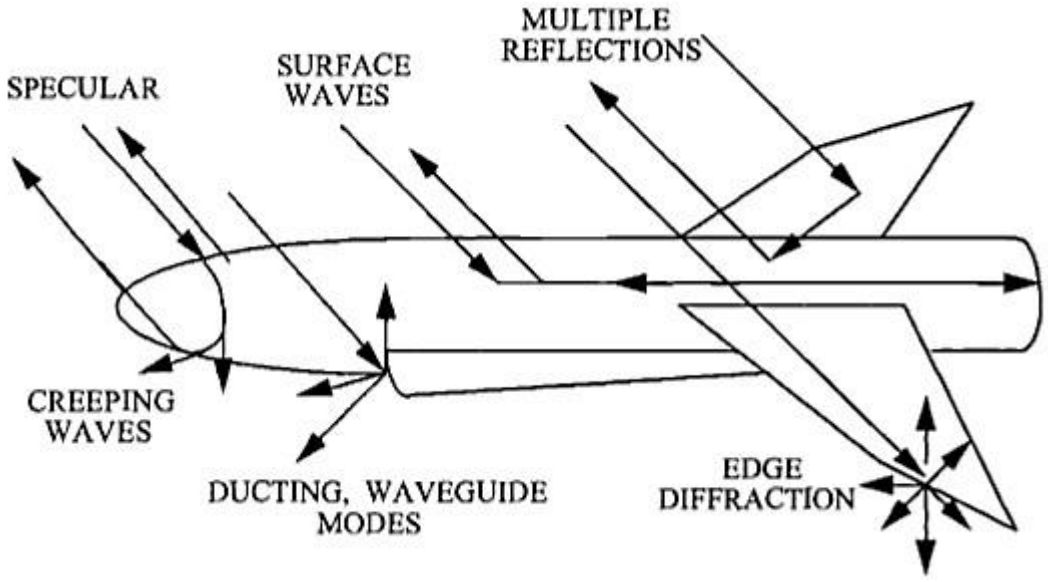

Figure 13: Illustration of important scattering mechanisms *(4)*

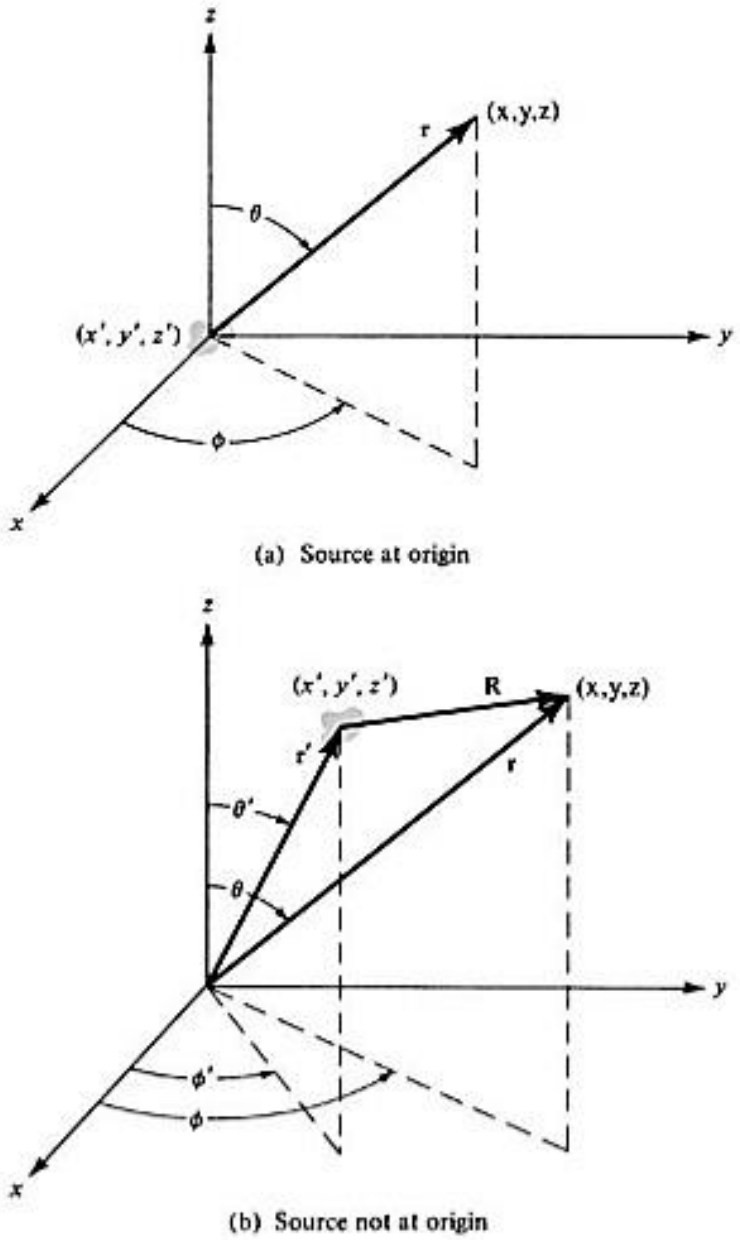

Figure 14: Coordinate system for computing fields radiated by sources *(6)*

Optimization

Optimization means finding such a solution to a problem subjected to certain constraints that bind the solution in a particular range. Optimization means finding the most suitable solution that satisfies the constraints placed on the given problem. The function that needs to be optimized is called the objective function.

Optimization may refer to a problem in which one function needs to be optimized. It may also refer to a problem involving more than one objective functions. Such a problem involving more

than one objective function is called a Multi-objective optimization problem. Optimization of a function can be done via several techniques. A few of them are:

Multi-objective optimization techniques are:

- Weighted sum approach
- e-Constraint method
- Goal programing
- Utility function method:
- Particle swarm optimization.
- Ant colony optimization:
- Tabu Search

Optimization method

1. Gradient Methods/ Model Based Approach

In model-based method, we have an equation or a set of equations that are subject to one or more than one constraint and are given some range in which the equations are to be used. Model based methods are relatively easier to optimize and conventional optimization software are effective in solving these optimization problems.

2. Search Methods/ Data Driven Approach

Data driven approach to optimization is only used when there is an unavailability of an explicit mathematical relationship between variables. When such a case arises, a large pool of data is collected. This data is then used to obtain an optimized solution.

Because here there is a large pool of data, the optimization software or algorithm needs to check each of these data points. This, in turn translates into higher computing cost, resource and time. There is an alternative approach to solving data driven problems, a novel and relatively new approach i.e. *evolutionary algorithms***.**

Genetic Algorithm

Genetic algorithm is a guided random search method. It is based on the Darwinian principle of survival of the fittest in natural selection. Genetic algorithm is an artificial reproduction of the genetic process that promotes the selection of favorable characters or traits from amongst the genes in a generation.

Genetic algorithm provides a favorable alternative which is not computationally as intensive as the conventional algorithm. In GA, one works with a population of points rather than a single

point. The fitness (value of the objective function) of each individual in the population (corresponding to a point in the search space) is then computed. Individuals who have high fitness value undergo crossover and mutation with the hope that they produce better offspring. By better offspring, we mean that they have higher fitness value as compared to their parents.

In genetic algorithm, we have an initial set of population. This set is used to find the values of the objective function. The values out of the initial population that give a result that is closer to the desired outcome are saved while the rest of the less-favored elements in the initial population are left behind. In the next iteration (called generation), the favored values undergo cross over and mutation to help improve their outcome values. This, therefore ensures that the coming generation will have more favorable characteristics than the parents i.e., the result of the next generation will be closer to the optimum value than the parent generation.

In this project, Multi-Objective Optimization is performed using GA due to the following reasons (8):

1. GA is a data-driven approach. It does not require gradient information. It can be effective regardless of the nature of the objective function.
2. GA is a global optimization technique, which means it converges to a global solution rather than local solution.
3. Multi-Objective GA was available in MATLAB Optimization Toolbox (a variant of NSGA-II (9)) which saved us from the formidable task of programming one ourselves and reduced the chances of error.
4. Since, the optimization algorithm was data-driven, this allowed us to use proven software for aerodynamic and RCS computations which could be coupled with MATLAB optimization toolbox.

Some of the important terminologies associated with genetic algorithms are

Crossover

In cross over, different genes from a chromosome are exchanged between two chromosomes. This exchange produces new iterations in the sample of population. The newly produced chromosome (input value in binary form) may produce better results or worse than the parent chromosome.

In mathematical and computational terms, each gene is a number in binary form. A chromosome is an array of binary numbers. During cross over, some part of a binary chromosome is cut from one and is burned on to the other chromosome.

Mutation

In order to ensure that the population maintains diversity, a process called mutation occurs. In mutation, the algorithm automatically choses a random location of a gene and changes it i.e., if it were a 1, it will be changed to 0 and if it were a 0, it will be changed to 1. Mutation has very low probability.

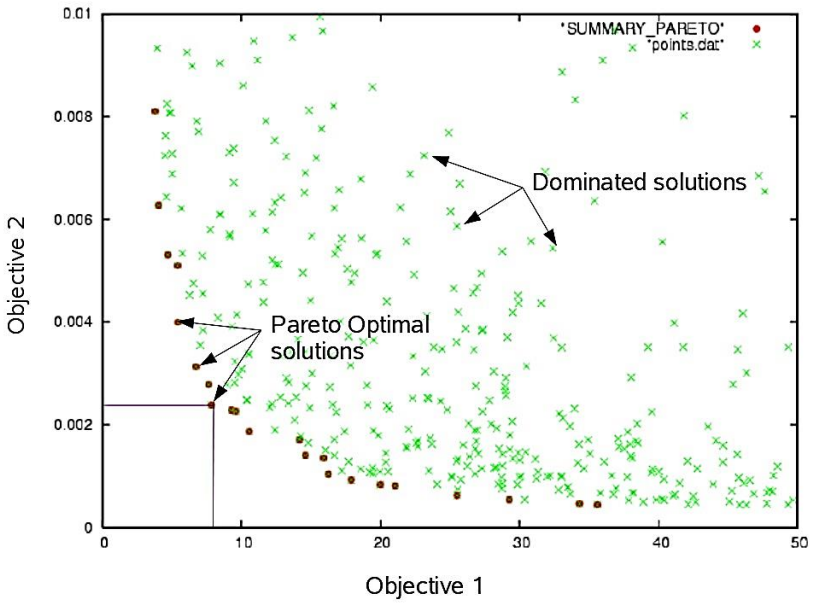

Figure 15: An example of Criterion Space

Pareto front represents a number of points which given optimized solution to the given problem. In some cases, Pareto front is easy to visualize while it is nearly impossible to visualize in other cases.

CHAPTER 3: METHODOLOGY

To begin with, a mission profile was developed to ascertain design goals, the concept design phase was commenced by selection of proven stealth UCAVs, out of which one was to be selected as baseline for optimization process. Since the goal of this optimization process is maximizing lift to drag ratio and minimizing RCS, the criterion for selection was best aerodynamic performance and least radar signature. The geometry of the baseline aircraft was parameterized in order to reduce the number of design variables using Class Shape Transformation (CST) Technique. With parameterized geometry, the airfoil and planform of X47B underwent optimization, with Lift to drag ratio (L/D) and RCS as Objective Functions under chosen design conditions, using Multi Objective Genetic Algorithm (GA), coupled with Higher Order Panel Method code Athena Vortex Lattice (AVL) and RCS Calculation Software POFACETS.

Mission Profile

As with any product, the design is to stem from the operational requirements, so the first element is to ascertain the **Mission Profile**, which consists of the mission that the aircraft is required to undergo. All the climbs, cruises, loiters, turns, rolls, pulls etc. are required to be noted down. These abstract requirements, are then translated into limits of operational Altitudes, Speeds, Range, Rate of Climb requirements.

For this, the Close Air Support (CAS) strategy was studied, and efforts were made to amalgamate the CAS strategies, with modern 5^{th} generation warfare concepts, relying on extensive networking, communication and integration between battlefield systems. The following mission profile was devised as a result.

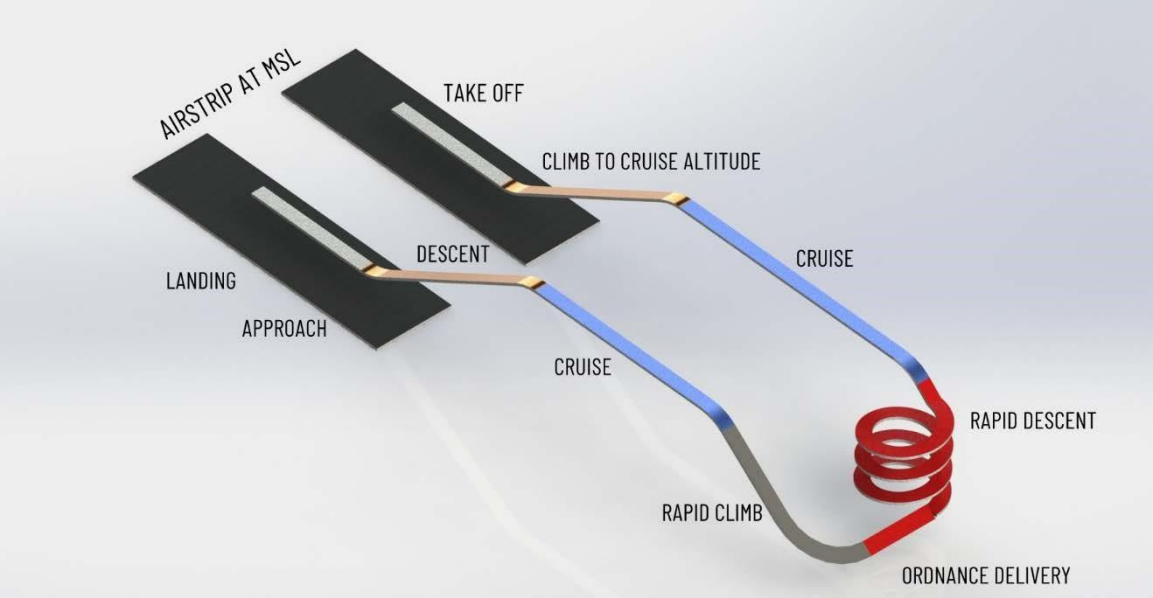

Figure 16: Mission Profile

Technical Performance Measures (TPMs)

These figures from the mission profile were then be translated into concrete figures depicting the required Aircraft performance parameters and stability figures, which are collectively known as Technical Performance Measures (TPMs).These were ascertained to be as follows.

Maximum Take-off Mass, MTOM	6.5 Kg
Bank angle at maximum Load Factor, θ_{MAX}	60 Degrees
Rate of Climb,ROC	792 $ftmin^{-1}$
Take-off Speed, V_{TO}	19.55 ms-1
Take-off Run, S_{TO}	250 m
Sustained Turn Speed, $V_{SUSTURN}$	28 ms^{-1}
Maximum Speed, V_{MAX}	35 ms^{-1}
Stall Speed, V_{STALL}	17 ms^{-1}
Service Ceiling, h_{SC}	1200 m MSL

Constraint Analysis

The resulting TPMs gave us the design objectives, around which the concept design is going to be based on. These parameters were then used as constraints to draw up graphs of the aircraft's

performance at all possible variations of Wing Loading W/S versus Thrust to Weight Ratio T/W. For this the following equations (10) were employed. These equations are derived using equation of motion for every flight condition. Interested readers can see reference (10) for derivations.

T/W for a Level Constant-velocity Turn

$$\frac{T}{W} = q\left[\frac{C_{D\min}}{(W/S)} + k\left(\frac{n}{q}\right)^2\left(\frac{W}{S}\right)\right]$$

T/W for a Desired Specific Energy Level

$$\frac{T}{W} = q\left[\frac{C_{D\min}}{(W/S)} + k\left(\frac{n}{q}\right)^2\left(\frac{W}{S}\right)\right] + \frac{P_S}{V}$$

T/W for a Desired T-O Distance

$$\frac{T}{W} = \frac{V_{LOF}^2}{2g\cdot S_G} + \frac{q\cdot C_{D\ TO}}{W/S} + \mu\left(1 - \frac{q\cdot C_{L\ TO}}{W/S}\right)$$

T/W for a Desired Rate of Climb

$$\frac{T}{W} = \frac{V_V}{V} + \frac{q}{(W/S)}C_{D\min} + \frac{k}{q}\cdot\left(\frac{W}{S}\right)$$

T/W for a Desired Cruise Airspeed

$$\frac{T}{W} = qC_{D\min}\left(\frac{1}{W/S}\right) + k\left(\frac{1}{q}\right)\left(\frac{W}{S}\right)$$

T/W for a Service Ceiling (ROC = 100 fpm or 0.508 m/s)

$$\frac{T}{W} = \frac{V_V}{\sqrt{\frac{2}{\rho}\left(\frac{W}{S}\right)\sqrt{\frac{k}{3\cdot C_{D\min}}}}} + 4\sqrt{\frac{k\cdot C_{D\min}}{3}}$$

The resulting graphs of the aforementioned equations were plotted simultaneously in Microsoft Excel, to determine the design point, which is the point with the least Wing-Loading and Thrust to Weight Ration that satisfies the operational requirements.

The plot comes out to be as follows:

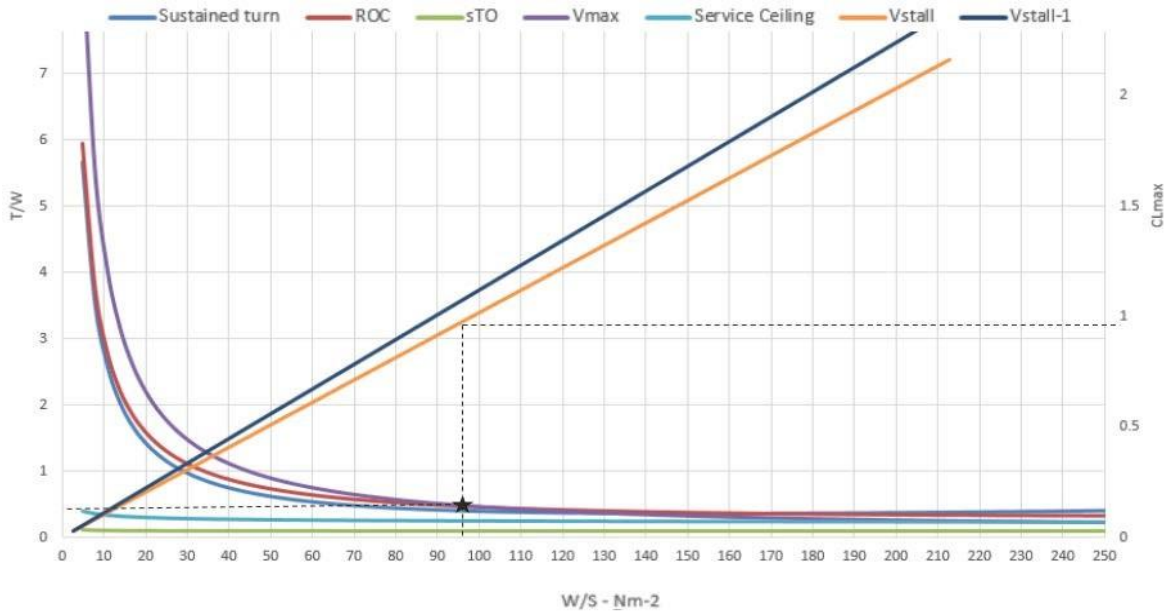

Figure 17: Constraint Diagram

From the design point we can extract the following information:

1. Wing-Loading $\left(\frac{W}{S}\right)$- 97 N/m^2
2. Required Wing Reference Area - $S = \frac{W}{W/S} = 0.67\ m^2$
3. Maximum Coefficient of Lift required for Takeoff- $C_{Lmax} = 1$

Preliminary Airfoil selection

The next step in the design process is to select an Airfoil. The requirements for the airfoil can be translated from the results of the Constraint Analysis design point by means of the following equations (1).

Aircraft Cruise Lift Coefficient	$C_{Lc} = \frac{2W_{ave}}{\rho {V_c}^2 S}$
Aircraft Wing Cruise Lift Coefficient	$C_{Lc\,W} = \frac{C_{Lc}}{0.95}$
Ideal Lift Coefficient	$C_{Li} = \frac{C_{Lc\,W}}{0.95}$
Aircraft Max lift Coefficient	$C_{Lc} = \frac{2W_{TO}}{\rho {V_c}^2 S}$
Wing Max Lift Coefficient	$C_{Lmax\,W} = \frac{C_{Lmax}}{0.95}$

Where;

W_{ave} Average Aircraft Weight

C_{Lc} Cruise Lift Coefficient

V_c Cruise speed

S Reference Area

ρ Air density

C_{LCw} Wing Cruise Lift Coefficient

W_{TO} Take-off Weight

C_{Lmax} Max Lift Coefficient

Solving the aforementioned equations gives airfoil requirements

Table 4: Required Airfoil Coefficients

Aircraft Cruise Lift Coefficient	C_{Lc}	0.18267
Wing Cruise Lift Coefficient	C_{Lcw}	0.18267
Wing Ideal Lift Coefficient	C_{Li}	0.20297
Aircraft Max Lift Coefficient	C_{Lmax}	0.49555
Aircraft Gross Lift Coefficient	C_{LmaxG}	0.55062

The next step was to select an airfoil that satisfied the requirements as above, following criteria was developed for the selection.

Table 5: Airfoil Selection Criteria

C_{lmax}	Maximum Lift Coefficient	Maximum
α_{Stall}	Stall angle	Maximum, with gradual onset
C_{dmin}	Minimum Drag coefficient	Minimum
C_{lalpha}	Lift-Curve Slope	Maximum
$C_{m'inc}$	Pitching moment coefficient corresponding to cruise	Minimum
C_{mo}	Pitching moment coefficient corresponding to $\alpha=0°$	Minimum
$C_{m'max}$	Pitching moment coefficient corresponding to maximum allowable α	Minimum

$C_{L\alpha max}$	C_L corresponding to maximum allowable α	Maximum
$C_L/C_{d\ max}$	Maximum Lift-drag ratio	Maximum
$\alpha_{CL/Cd\ max}$	AOA corresponding to $C_L/C_{d\ max}$	Minimum
Range of Operation (α_{max} - α_{min})	Range of operation corresponding to acceptable variation in drag	Maximum

Numerous airfoils were analyzed, constituting the following series:

1. NACA 4 digit airfoils
2. NACA 5 digit airfoils
3. NACA 6 series
4. Wortmann
5. Martin Hepperle
6. Selig

Data was extracted from the airfoil plots from (11) to provide the basis of comparison along the lines of the aforementioned matrix measures of merit.

Table 6: Airfoil Selection Matrix

	Sellig	***Wortmann***		***Martin Hepperle***			
ID	**S1223**	**FX L V-152**	**FX V 60-100**	**MH-60**	**MH-61**	**MH-62**	**MH-64**
α_o	-7	0	-4.8	-1	-0.05	-1	-1.8
C_{lo}	1.2	0	0.5	0.1	0.1	0.12	0.17
C_{lmax}	2.25	1.15	1.62	1.1	1	1.1	1.07
α_{Stall}	12.5	15	12.5	12	10	10	10
C_{dmin}	0.015	0.007	0.0068	0.01	0.007	0.007	0.007
C_{lalpha}	0.1052	0.1	0.1	0.1	0.09	0.1	0.1
$C_{m'inc}$	-0.27	-0.00333	-0.12	-0.011	-0.00667	-0.015	-0.017
C_{mo}	-0.27	-0.00167	-0.12	-0.02	-0.015	-0.025	-0.022
$C_{m'max}$	-0.27	-0.015	-0.12	-0.35	-0.03	-0.03	-0.022
$C_{L\alpha max}$	2.2	1	1.52	1.18	0.9	1.1	0.95
$C_L/C_{d\ max}$	85	50	112	70	70	70	70

$\alpha_{CL/Cd\ max}$	5	5	3	5	5	5	5
α_{min}	-2	-10	-5	-5	-5	-5	-5
α_{max}	10	10	10	10	8	10	8

The best airfoil out of the ones narrowed down, evidently came out to be the ***Wortmann FX L V152***, which then moved on as the basis for the concept, which is to undergo optimization.

Concept Design

The concept design process was to entail narrowing down of existing aircraft that come close to satisfying the TPMs. Upon research they were identified as:

1. Boeing X-45-B
2. Boeing X-45-C
3. Northrop Grumman X-47-A
4. Northrop Grumman X-47-B

Sizing and CAD Modeling of Baselines

These potential baseline aircrafts were then modelled in a 3D CAD Software, namely Solidworks, scaled up to the Reference Area resulting from the constraint analysis.

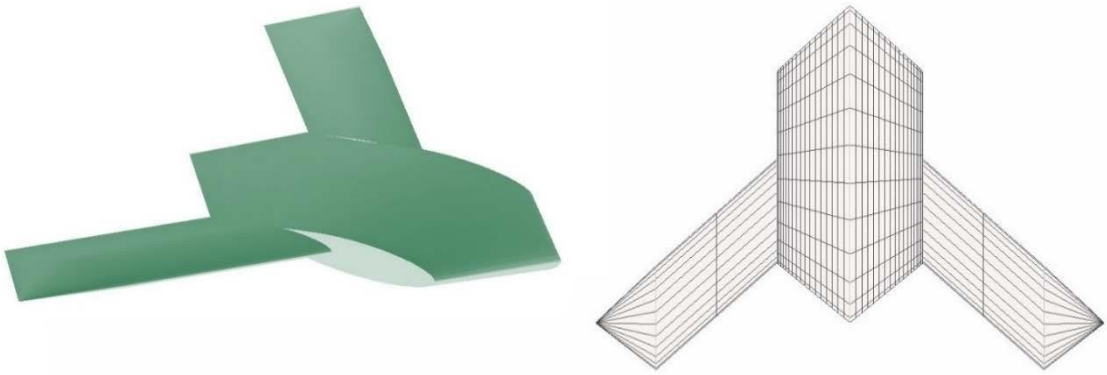

Figure 18: Boeing X-45A

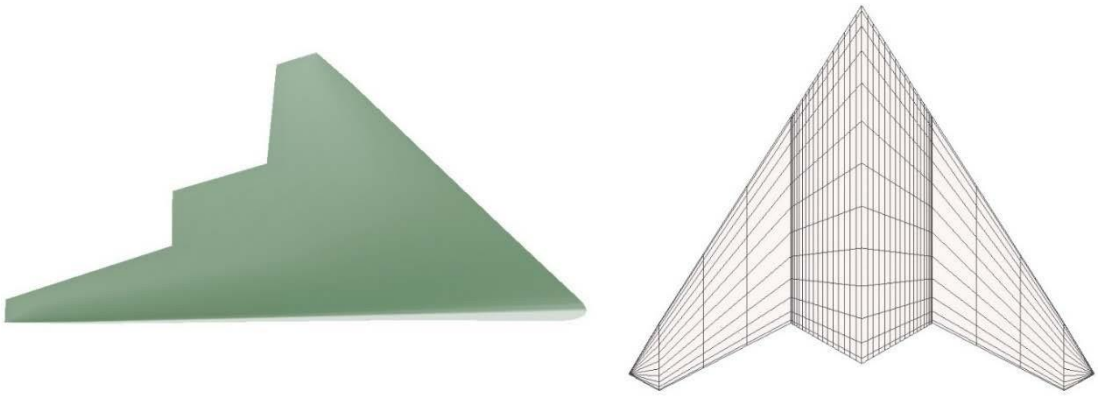

Figure 19: Boeing X-45C

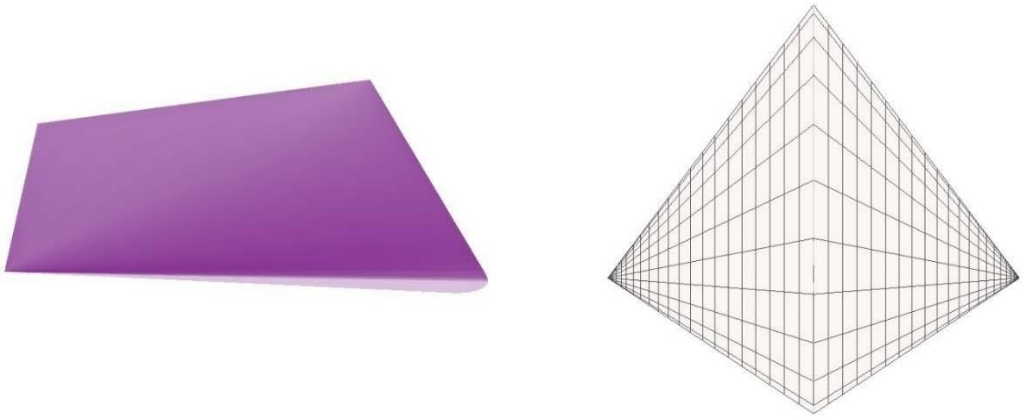

Figure 20: Northrop Grumman X-47A

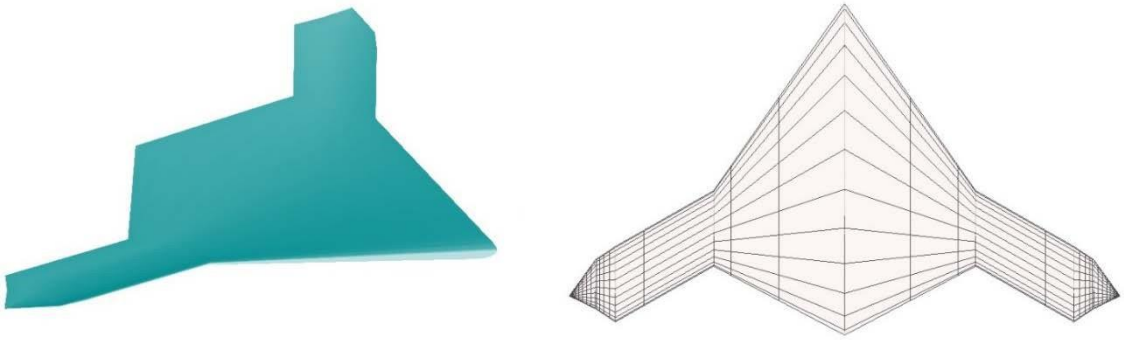

Figure 21: Northrop Grumman X-47B

Aerodynamic Analysis of Potential Baselines

The potential baselines underwent extensive analyses with respect to both RCS and Aerodynamic performance. For the Aerodynamic Analysis, XFLR-5, which is a Low Fidelity Computational Fluid Dynamics (CFD) software based on the Panel Method, was used.

The first step was modeling each aircraft's geometry in XFLR5, followed by input of Aircraft weight, inertia, operating conditions (Altitude, Speed, Angle of Attack etc.). The analysis type was selected as VLM (Vortex Lattice Method), of the Horse-shoe Vortex type. Moreover, Inviscid conditions was be assumed, since the operating speed of the aircraft is expected to be in the incompressible regime.

The results of the analysis provided graphs of the following parameters:

1. Lift Coefficient - C_L
2. Drag Coefficient – C_D
3. Pitching Moment Coefficient – C_M
4. Lift to Drag Ratio $\frac{L}{D}$ or $\frac{C_L}{C_D}$

Results of Aerodynamic Analysis

The analysis in XFLR5 yielded the following graphs:

Boeing X-45B

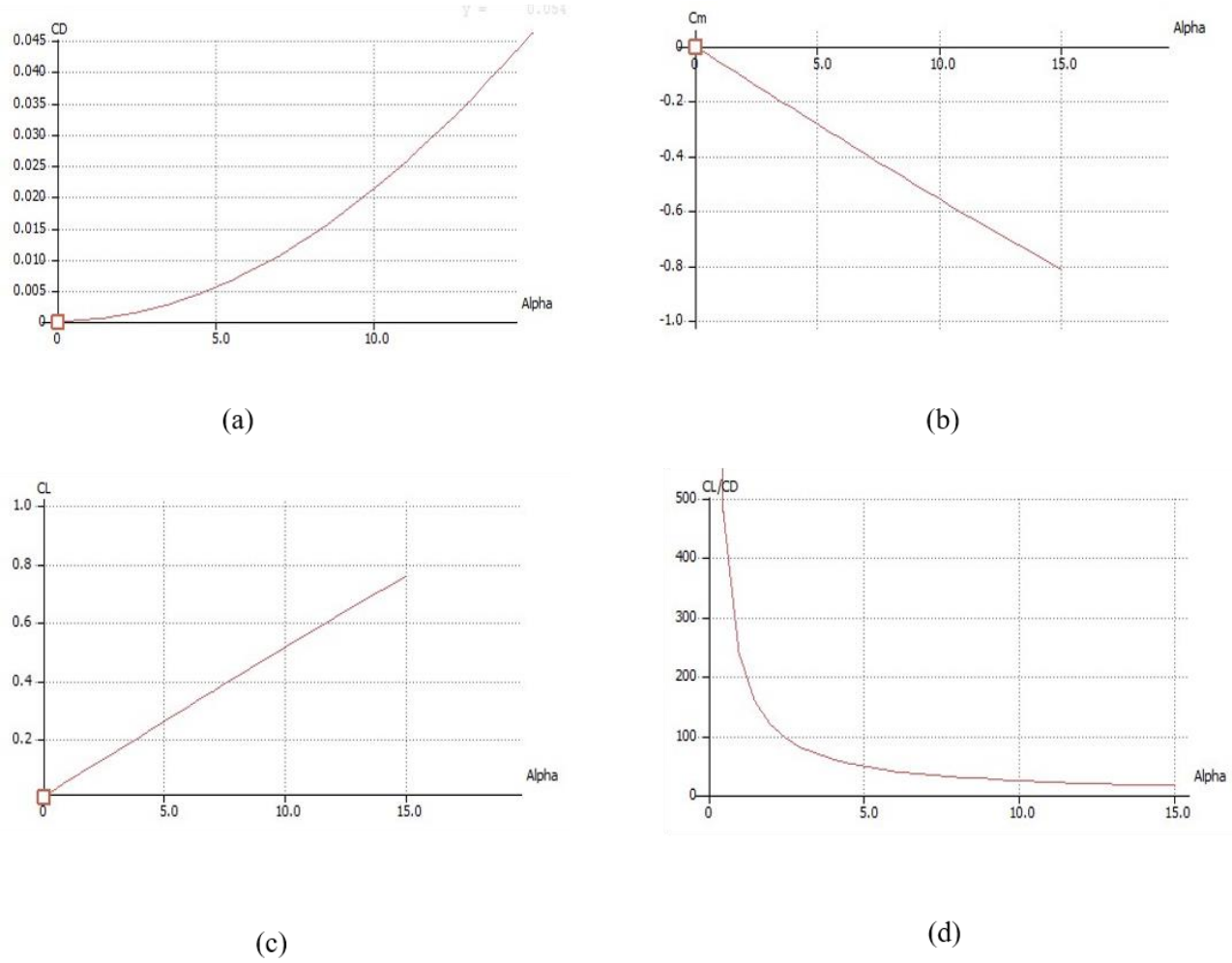

Figure 22: Boeing X-45B (a) CD vs α (b) Cm vs α (c) CL vs α (d) CL/CD vs α

Boeing X-45C

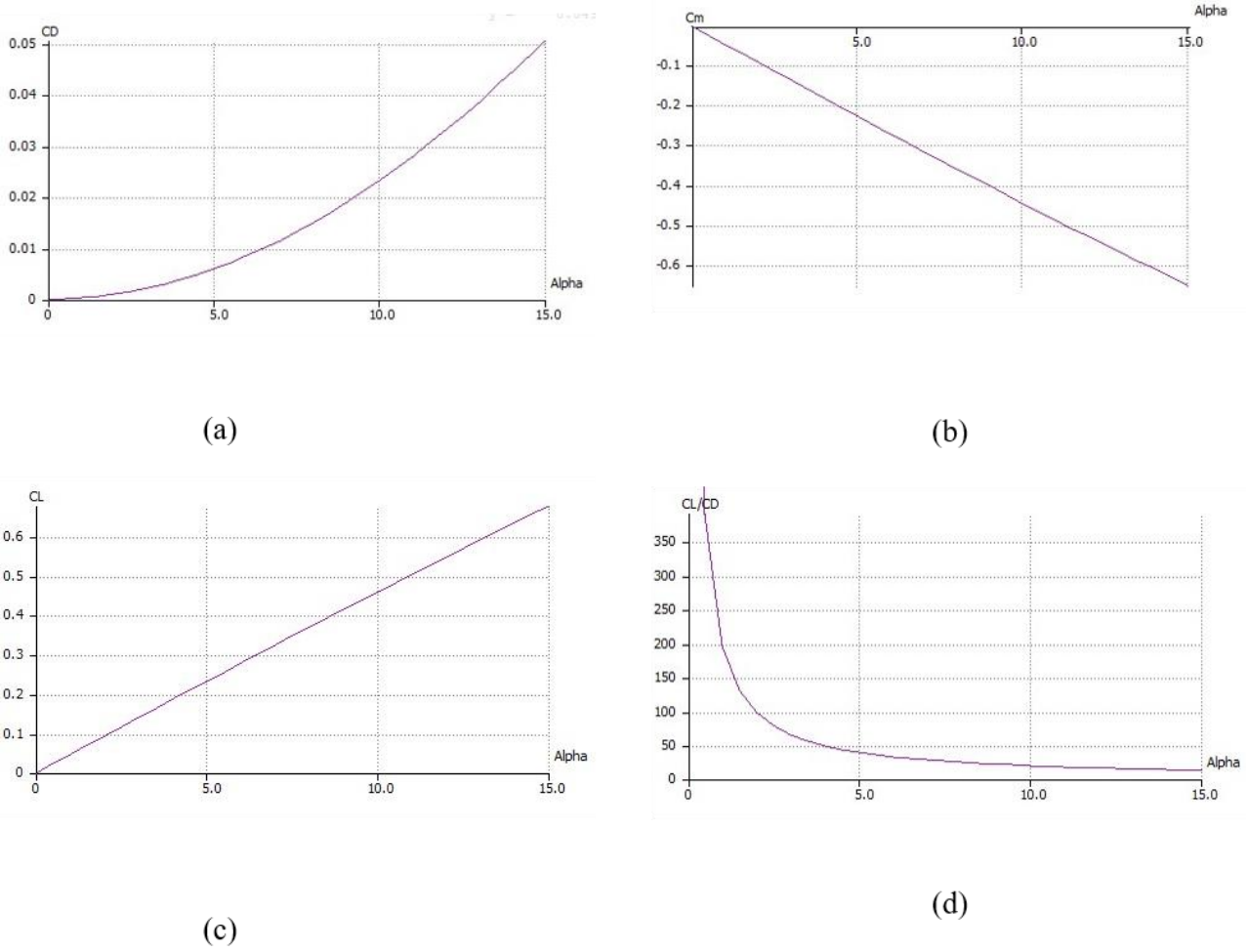

Figure 23: Boeing X-45C (a) CD vs α (b) Cm vs α (c) CL vs α (d) CL/CD vs α

Northrop Grumman X-47A

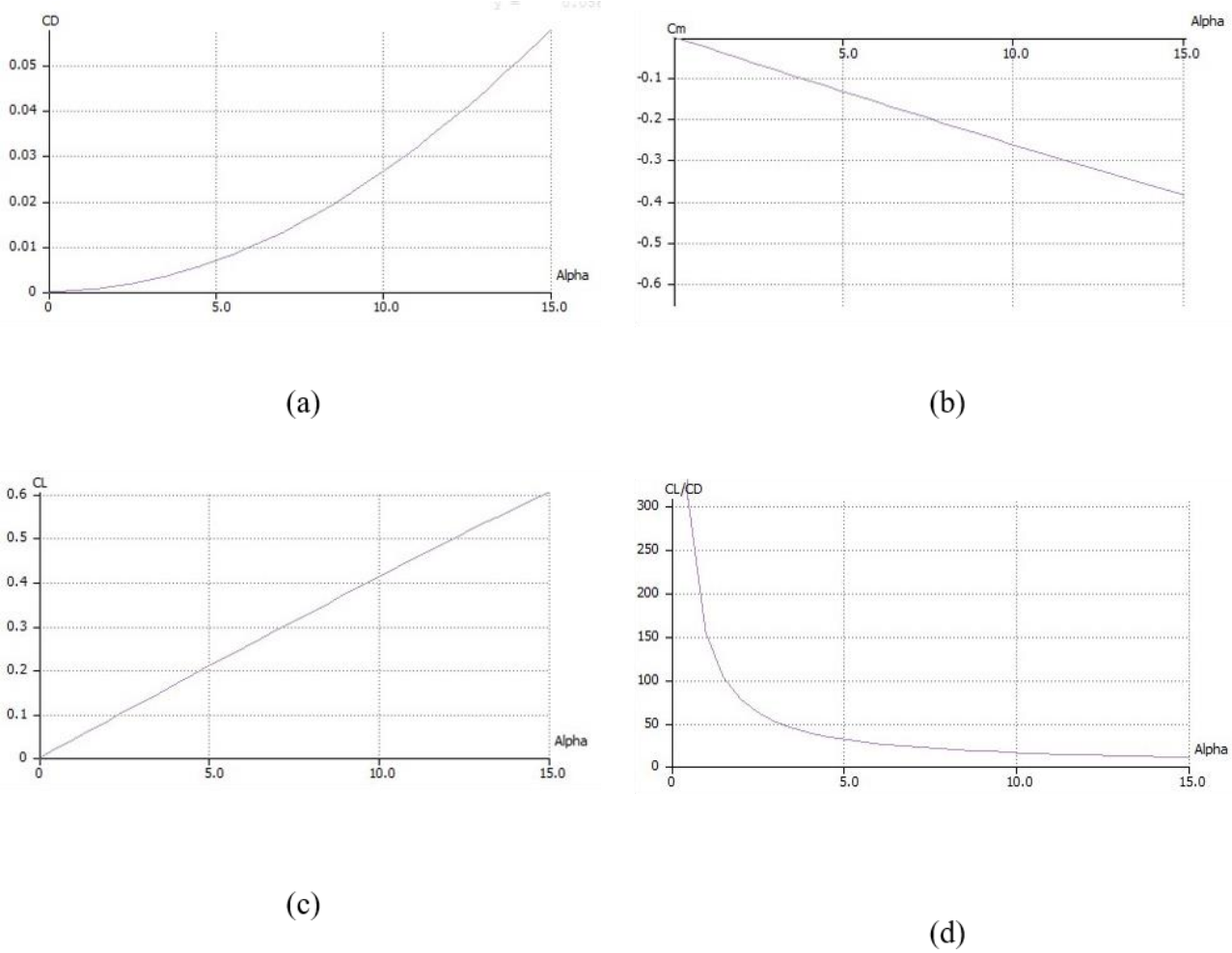

Figure 24: Northrop Grumman X-47A (a) CD vs α (b) Cm vs α (c) CL vs α (d) CL/CD vs α

Northrop Grumman X-47B

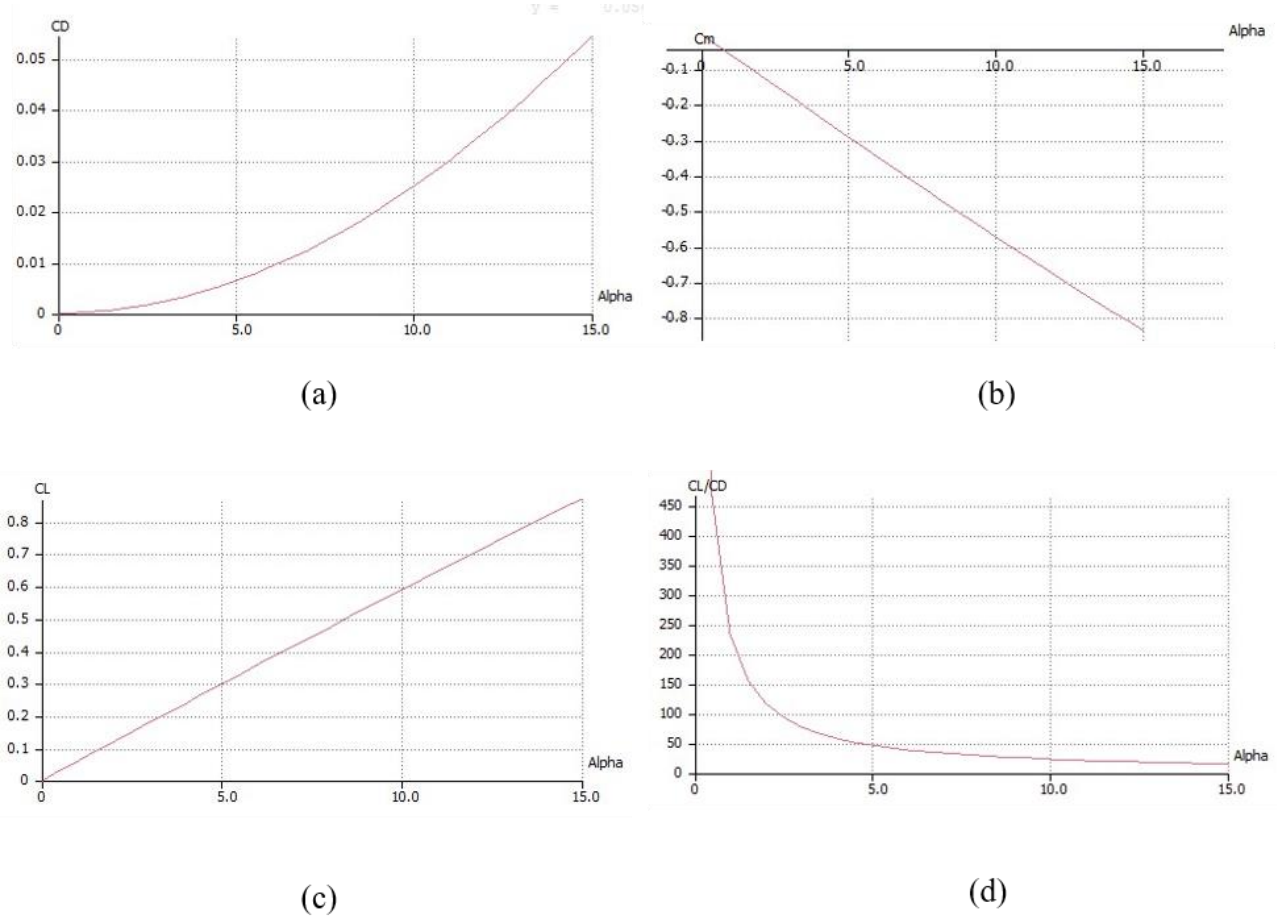

Figure 25: Northrop Grumman X-47B (a) CD vs α (b) Cm vs α (c) CL vs α (d) CL/CD vs α

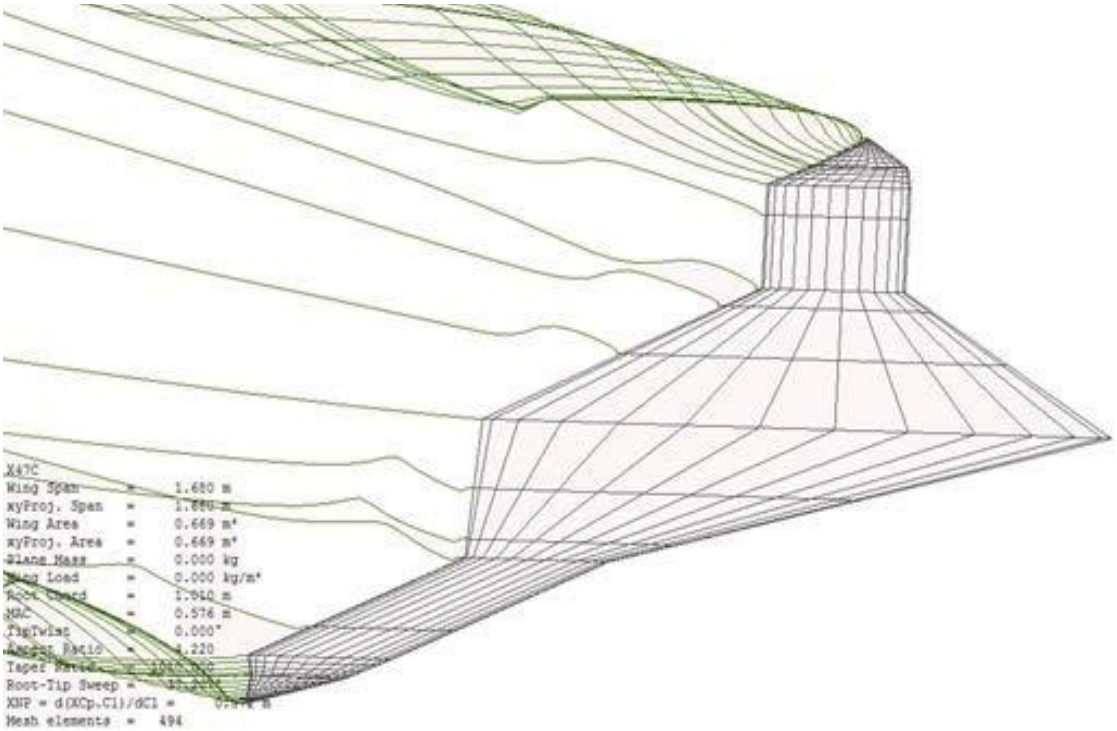

Figure 26: A visualization of the flow around the X-47B in XFLR5

The final data extracted from the graphs plotted as a result of the XFLR-5 VLM Aerodynamic analysis is tabulated as below

Table 7: Results of Aerodynamic Analysis

		X45B	***X45C***	***X47A***	***X47B***
$C_{m'max\text{-}AC}$	Max Aircraft C_m	-0.81	-0.645	-0.38	-0.833
$C_{d'max\text{-}AC}$	Max Aircraft C_d	0.046	0.0505	0.058	0.054
$CL_{max\text{-}AC}$	Max Aircraft C_L	0.757	0.677	0.603	0.87
α_{Cli}	α for Ideal C_L	4.05	4.52	5.05	3.5
C_{di}	C_D at α_{Cli}	0.0035	0.0048	0.0067	0.0031
$C_{m'i}$	C_m at α_{Cli} `	-0.226	-0.2	-0.133	-0.2
α_{CLmaxG}	α for Max Gross C_L	10.76	12.06	13.58	9.33
$C_{d,ClmaxG}$	C_D at α_{CLmaxG}	0.024	0.033	0.048	0.022
$C_{m'ClmaxG}$	C_m at α_{CLmaxG}	-0.595	-0.53	-0.35	-0.53

RCS Analysis

POFACETS 4.4.1 is a MATLAB routine for a 'first cut approximation' of RCS using Physical Optics Principle (12). It uses discretized model of a complex target body in the form of triangulations called 'facets' as input. Total scattered electric field can be written as a superposition of electric fields scattered from individual facets:

$$\left|\vec{E}_s\right| \approx \left|\sum_{n=1}^{N_S} \vec{E}_{s_n}\right|$$

$$\left|\vec{E}_s\right|^2 \approx \left|\sum_{n=1}^{N_S} \vec{E}_{s_n}\right|^2 \approx \sum_{n=1}^{N_S} \left|\vec{E}_{s_n}\right|^2$$

Then, from

$$\sigma \approx \sigma_1 + \sigma_2 + \cdots + \sigma_{N_S}$$

where N_s is the number of scattering sources. All these terms are a function of angle

(azimuth, φ and elevation θ) and frequency. The spherical coordinate system used for RCS calculation is shown in figure 27. POFACETS creates RCS plots as a function of azimuth and elevation angles

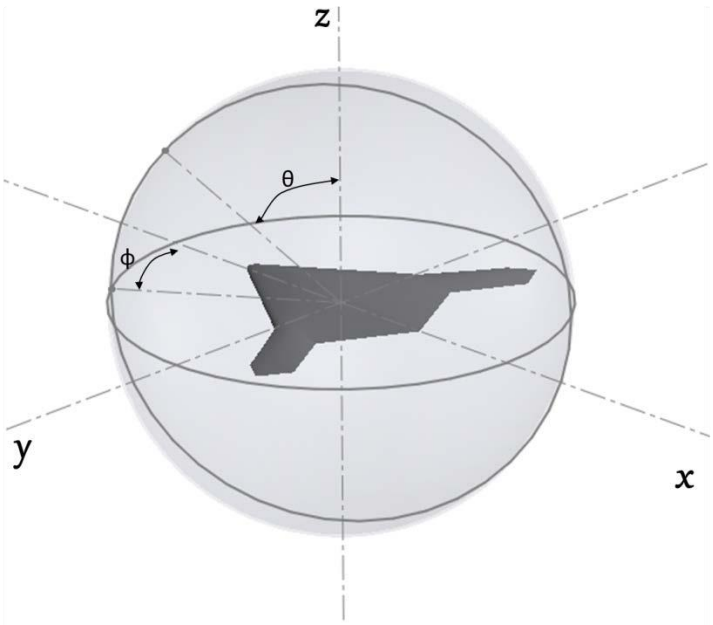

Figure 27: Spherical Coordinate System for RCS analysis

Calculation of RCS

The faceted geometries of potential baselines are shown in Figure 28.

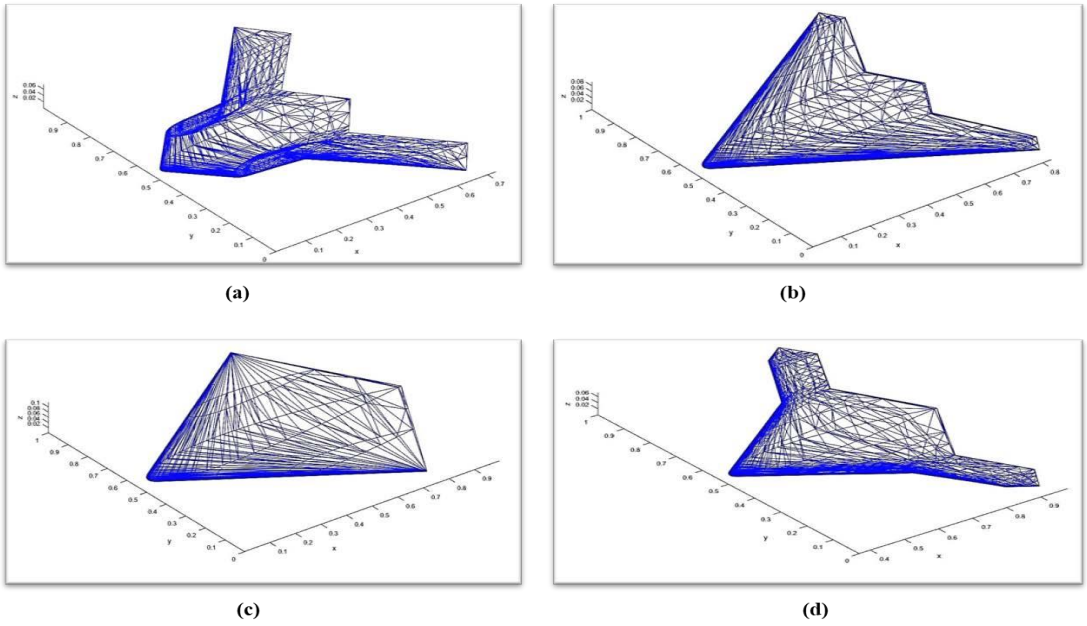

Figure 28 Discretized Models of Potential Baselines, (a) X-45B (b) X-45C (c) X-47A (d) X-47B

The Radar Cross Sections of these four aircraft were calculated at θ = 90 degrees with respect the coordinate system of figure 27, with varying azimuth angles (the so called "theta cut"). L-band frequency was used because of its wide usage. TE_z polarized electromagnetic waves are disturbed by ground effect, TM_z polarization is used instead. Since this was a comparative analysis, Perfect Electric Conductor was assumed as the target material. The Polar Graphs which show RCS as a function of azimuth angle are shown in Figure 29.

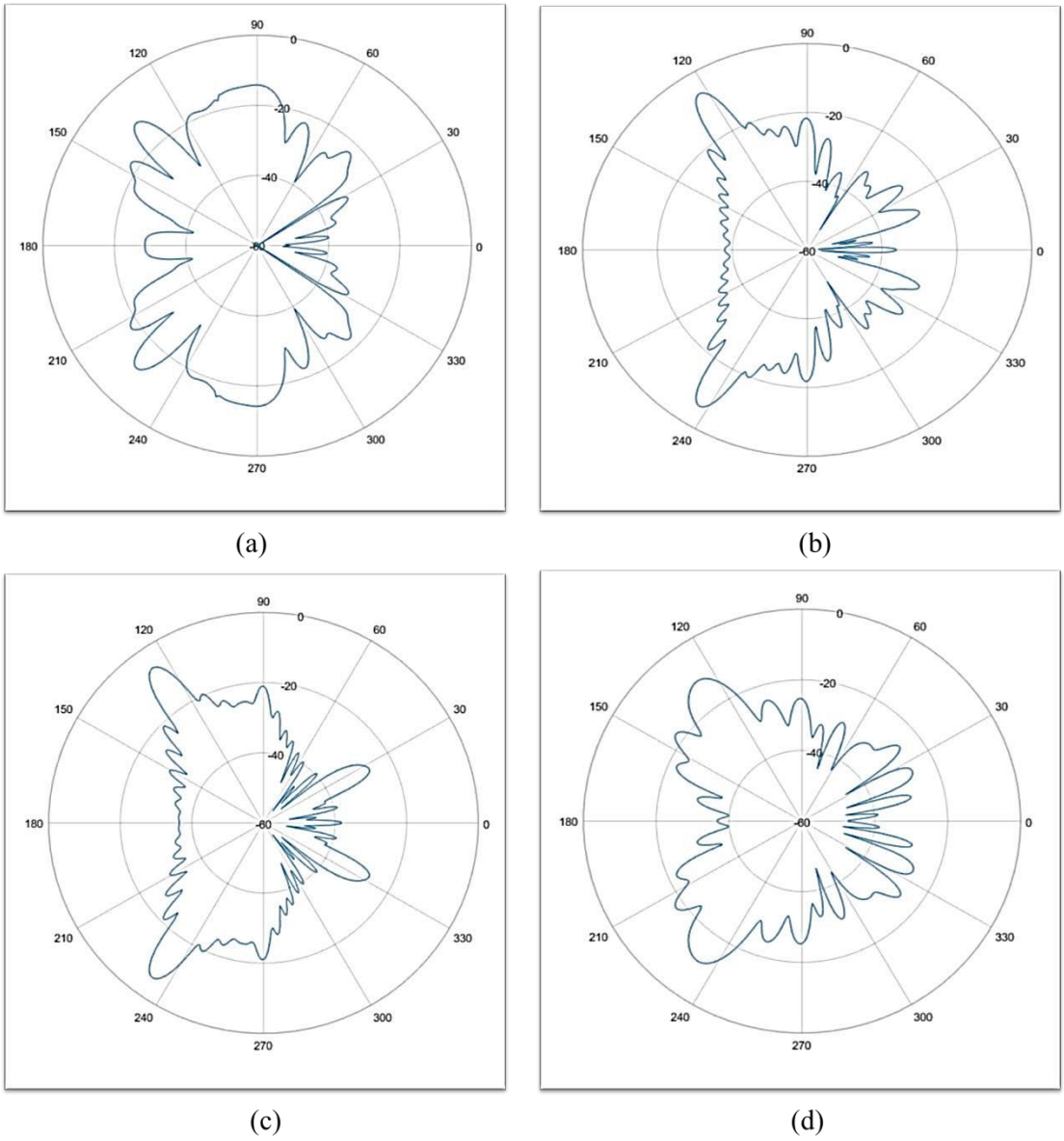

Figure 29: RCS as a function of Azimuth angle, theta = 90, L-band, TMz polarization

Parameterization

To save the computational expense, it was necessary to reduce the number of variables. Parameterization served this job.

Airfoil Definition

Two parameterization schemes for airfoil geometry representation and control were considered: Class Shape Transformation (13) and PARSEC (14).

Class Shape Transformation (CST)

The airfoil geometry can be defined with the help two functions namely class function, which specifies the class of aerodynamic body (e.g. airfoil, projectile, ellipse) and shape function which specifies the shape of that particular class. Trailing edge thickness can also be incorporated, but in the present case, it is set equal to zero. Following mathematical expressions show how CST works.

If $\psi = \mathrm{x}/\mathrm{c}$ and $\zeta = z/\mathrm{c}$ are the non-dimensional airfoil coordinates then, class function is defined as

$$C_{N2}^{N1} = \psi^{N1}[1-\psi]^{N2}$$

The class of aerodynamic body can be changed by varying N1 and N2, as table 8 shows.

Table 8: Working of Class Function

N1	N2	Class of Aerodynamic body
0.5	1.0	Rounded nose, pointed aft airfoil
0.5	0.5	Ellipse or ellipsoid
1.0	1.0	Pointed nose, Pointed aft end airfoil
0.75	0.75	Sears-Haack body
0.75	0.25	Low drag projectile
1.0	0.001	Cone or wedge airfoil
0.001	0.001	Rectangle

Shape function is expressed using Bernstein Polynomial (13) of order 'n'. From experience, a third order Bernstein Polynomial is good enough to approximate airfoil geometry accurately. For upper surface of airfoil, overall shape function is expressed as:

$$S_u(\psi) = \sum_{i=1}^{n} A_{u_i} . S_i(\psi)$$

The Component Shape Function is defined as:

$$S_i(\psi) = \frac{n!}{i!\,(n-i)!} . \psi^i . (1-\psi)^{n-i}$$

Finally,

$$\boldsymbol{\zeta_U = C_{N2}^{N1}(\psi) . S_U(\psi) + \psi \zeta_T}$$

Where, $\zeta_T = {}^{\Delta z_{TE}}/_{c}$ caters for the trailing edge thickness.

Putting everything together:

$$\boldsymbol{\zeta_U = \psi^{N1}[1-\psi]^{N2} . \sum_{i=1}^{n} A_{u_i} . \frac{n!}{i!\,(n-i)!} . \psi^i . (1-\psi)^{n-i} + \psi \zeta_T}$$

By looking at above equations, it is evident that one needs to play around with values of coefficients A_{u_i} and A_{l_i} to generate the desired airfoil shape. Use of an optimization technique can be helpful in such a case.

PARSEC

PARSEC expresses airfoil geometry as the following expressions.

$$y_u = \sum_{i=1}^{6} a_i x^{i-(1/2)}$$

$$y_l = \sum_{i=1}^{6} b_i x^{i-(1/2)}$$

Where, y_u and y_l are the y coordinates for the upper and lower surfaces respectively.

Eleven characteristics are defined for an airfoil: upper leading edge radius (R_{leu}), Lower leading edge radius (R_{lel}), Upper crest point (Y_{up}), lower crest point (Y_{lo}), Position of upper crest point (X_{up}), Position of Lower crest point (Xlo), upper crest curvature (YXX_{up}), Lower crest curvature (Y_{XXlo}), Trailing edge offset (T_{off}), Trailing edge thickness (TTE), Trailing edge direction angle (α_{TE}) and trailing edge wedge angle (β_{TE}) as shown in figure 30.

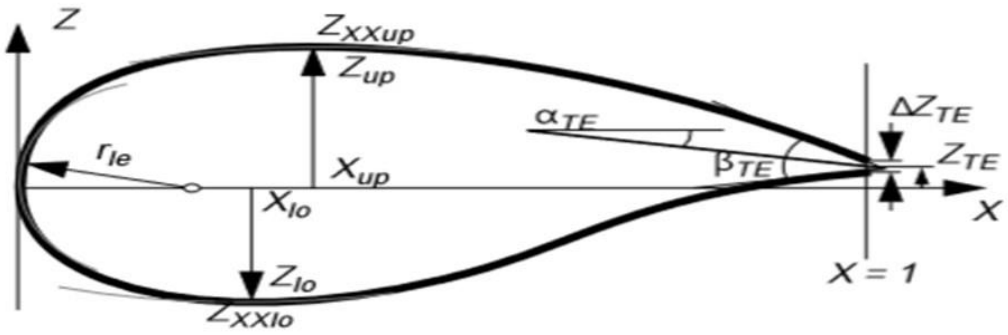

Figure 30 Airfoil defining parameters for PARSEC *(14)*

These characteristics are used to define the following conditions in order to solve for control variables a_i and b_i.

1. At x(u,l) = maximum, y(u.l) = maximum
2. At x(u,l) = maximum, $\frac{dy(u,l)}{dx} = 0$
3. At x(u,l) = maximum, $\frac{d^2y(u,l)}{dx^2} = maximum$
4. At $x_u = 1$, $y_u = T_{off} + \frac{T_{TE}}{2}$
5. At $x_l = 1$, $y_l = T_{off} - \frac{T_{TE}}{2}$
6. At $x_u = 1$, $\frac{dy_u}{dx} = \tan(\alpha_{TE} - \frac{\beta_{TE}}{2})$
7. At $x_l = 1$, $\frac{dy_l}{dx} = \tan(\alpha_{TE} + \frac{\beta_{TE}}{2})$

CST was chosen for parameterization because of three reasons:

1. Better accuracy
2. Fewer number of variables
3. Its ability to be extended in three dimensions without loss in consistency

Figure 31 shows a comparison of the two schemes**.**

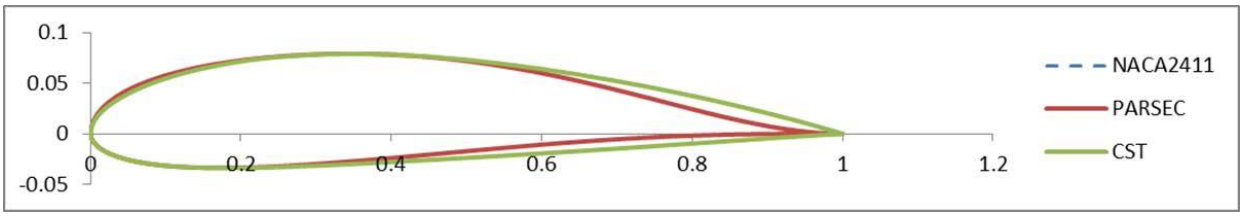

Figure 31: PARSEC and CST Comparison

3D Wing definition

CST can approximate many types of aerodynamic bluff bodies including airfoils, winglets, pylons, Nacelles, Fuselages and Wings. The 3D wing can be defined by distributing the airfoil sections across the wingspan. Here, two additional parameters namely wing shear distribution and twist angle distribution need to be specified, but in the present case, they are set equal to zero. The following mathematical expressions exploit the use of CST for 3D wing definition.

Fraction of local chord: $\psi = \frac{x - x_{LE}(\eta)}{c(\eta)}$

Non-dimensional semi-span station: $\eta = \frac{2y}{b}$

Local leading edge coordinates: $x_{LE}(\eta)$

Local chord length: c (η)

Non-dimensional upper surface coordinate: $\zeta_U(\eta) = \frac{z_U(\eta)}{c(\eta)}$

Non-dimensional local wing shear: $\zeta_N(\eta) = \frac{z_N(\eta)}{c(\eta)}$

$$\boldsymbol{\zeta_U(\psi,\eta) = C_{N2}^{N1}(\psi).\sum_{i=1}^{N_x}\sum_{j=1}^{N_y} B_{U_{ij}}.S_{y_j}(\eta).S_{x_i}(\psi) + \psi[\zeta_T(\eta) - tan\alpha_{TWIST}(\eta)] + \zeta_N(\eta)}$$

Where:

$$C_{N2}^{N1} = \psi^{N1}[1-\psi]^{N2}$$

$$S_{x_i}(\psi) = \frac{Nx!}{i!\,(Nx-i)!}.\psi^i.(1-\psi)^{Nx-i}$$

$$S_{y_j}(\psi) = \frac{Ny!}{j!\,(Ny-j)!}.\psi^j.(1-\psi)^{Ny-j}$$

Similarly,

$$\boldsymbol{\zeta_L(\psi,\eta) = C_{N2}^{N1}(\psi).\sum_{i=1}^{N_x}\sum_{j=1}^{N_y} B_{L_{ij}}.S_{y_j}(\eta).S_{x_i}(\psi) + \psi[\zeta_T(\eta) - tan\alpha_{TWIST}(\eta)] + \zeta_N(\eta)}$$

Coordinates of wing can be found as:

$$\boldsymbol{y = \frac{b}{2}\eta}$$

$$x = \eta C_{LOC}(\eta) + x_{LE}(\eta)$$

$$z_U(x,y) = \zeta_U(\psi,\eta)C_{LOC}(\eta)$$

$$z_L(x,y) = \zeta_L(\psi,\eta)C_{LOC}(\eta)$$

N_x and N_y represent orders of Bernstein Polynomial in x and y directions respectively. These xyz coordinates can be used to generate a surface using points having same chordwise and semi-spanwise coordinates joined together.

Airfoil Optimization

As a test case, NACA 2411 was optimized for maximizing Cl using Genetic Algorithm from MATLAB optimization toolbox. Figure 13 shows the algorithm used for this purpose. Upper and lower bounds were set as NACA 0021 and NACA 0004 respectively for which Bernstein Coefficients are as under.

	i= 1	**i = 2**	**i = 3**	**i = 4**	
$\mathbf{A_{ui}}$	0.295123	0.274268	0.235585	0.269459	**Upper Bound**
	0.056196	0.052343	0.044616	0.051729	**Lower Bound**
$\mathbf{A_{li}}$	-0.0562	-0.05234	-0.04462	-0.05173	**Upper Bound**
	-0.29512	-0.27427	-0.23558	-0.26946	**Lower Bound**

XFOIL

XFOIL is a FORTAN 77 code developed by Mark Drela of Massachusetts Institute of Technology in 1985 for airfoil analysis and design (15). It can perform viscous or inviscid analysis of existing airfoil, allowing:

- Forced or free transition
- Transitional separation bubbles
- Limited trailing edge separation
- Lift and drag predictions just beyond C_{lmax}

Optimization Algorithm

Figure shows the algorithm designed for optimization of NACA 2411 as a test case.

Inverse CST (16) represents finding the CST Coefficients with fourth order Bernstein Polynomial, using MATLAB optimization toolbox. Inverse CST involves using any optimization code to reduce the error between CST generated airfoil and airfoil coordinates in the Selig format airfoil coordinates (.dat) file. This makes a total of 8 design variables. MATLAB-XFOIL interface by Mr. Louis Edelman downloaded from MATLAB Central (17), was used for inviscid evaluation of C_L at 5 degrees angle of attack and coupled with CST such that both can be used with single standard input specified by user.

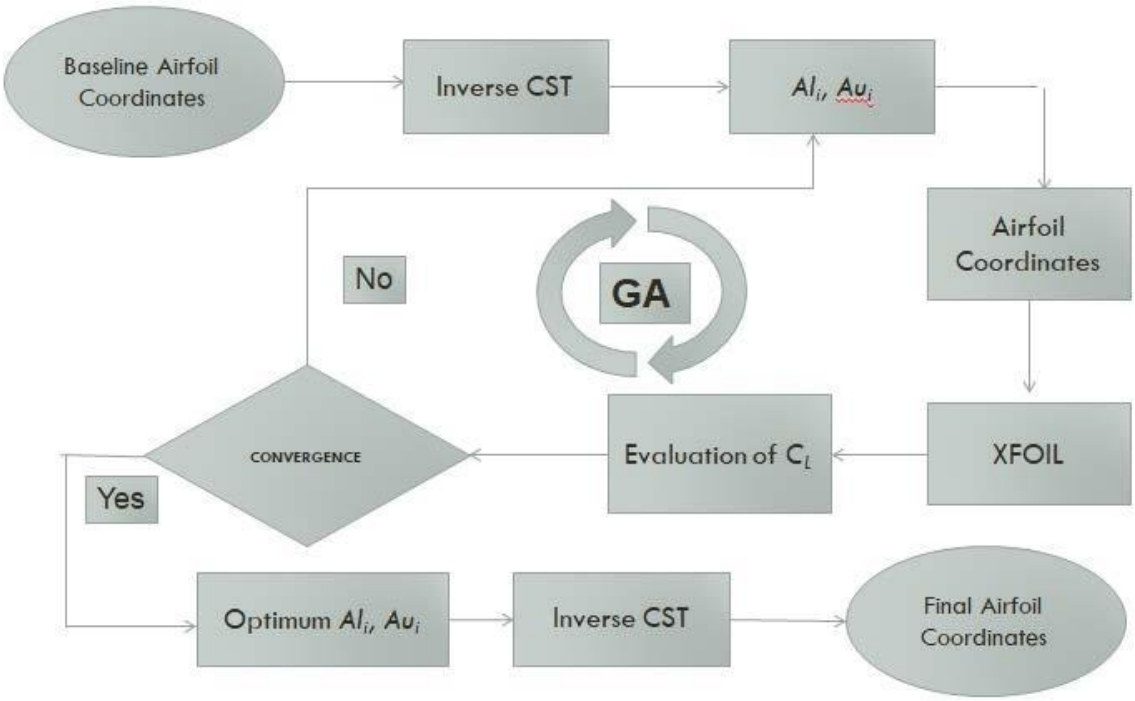

Figure 32: Airfoil Optimization Algorithm

Airfoil Optimization Results

Figure 33 shows an optimized airfoil generated as a result which clearly depicts higher camber of optimized airfoil as compared to baseline airfoil. Table 9 shows the optimization results

Table 9: Airfoil Optimization Results

Parameter	**Original Value**	**Optimized Value**
Lower Surface Coefficients	-0.1323, -0.0514, -0.0703, -0.0412	-0.0587, -0.0566, -0.0446, -0.0522
Upper Surface coefficients	0.1798, 0.2298, 0.1869 0.2231	0.2926, 0.2693, 0.2356 0.2671
Lift Coefficient at AOA $=5^0$	0.85	1.08

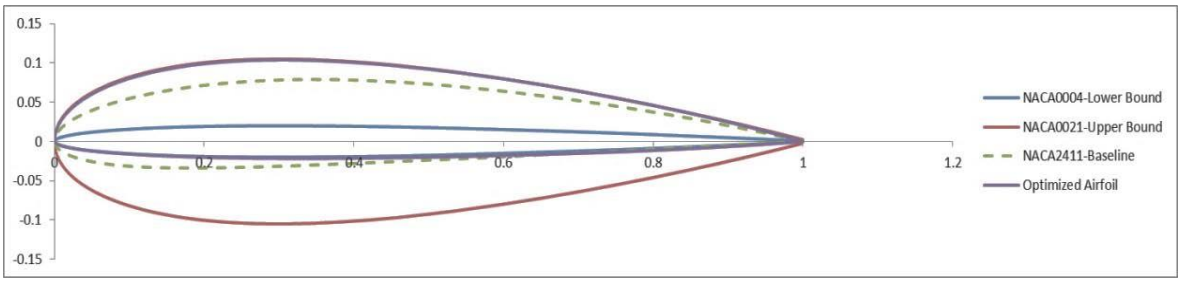

Figure 33: Airfoil Optimization Results

Selection of Baseline Design

A detailed comparison was then drawn on the basis of the results of Aerodynamic analysis along with the results of the RCS using the **Pugh Matrix**, which is a technique that gives weights to different TPMs and ranks them in accordance with their values to ascertain the ideal baseline which was then be used as an input for the Multi-objective optimization.

The final results of Aerodynamic and RCS Analysis are tabulated as below:

Table 10: Results of Aerodynamic and RCS Analyses

Characteristic	Description	X45B	X45C	X47A	X47B
$C_{m'max\text{-}AC}$	*Max Aircraft* C_m	-0.81	-0.645	-0.38	-0.833
$C_{d'max\text{-}AC}$	*Max Aircraft* C_d	0.046	0.0505	0.058	0.054
$C_{Lmax\text{-}AC}$	*Max Aircraft* C_L	0.757	0.677	0.603	0.87
α_{Cli}	*α for Ideal* C_L	4.05	4.52	5.05	3.5
C_{di}	C_D *at* α_{Cli}	0.0035	0.0048	0.0067	0.0031
$C_{m'i}$	C_m *at* α_{Cli}	-0.226	-0.2	-0.133	-0.2
α_{CLmaxG}	*α for Max Gross* C_L	10.76	12.06	13.58	9.33
$C_{d,ClmaxG}$	C_D *at* α_{CLmaxG}	0.024	0.033	0.048	0.022
$C_{m'ClmaxG}$	C_m *at* α_{CLmaxG}	-0.595	-0.53	-0.35	-0.53
RCS	*Radar Cross Section* (dBm^2)	-26.5059	-31.9289	-32.3776	-29.1272

The measures of merit were then assigned weightages and each value was then marked against a reference value to constitute the ranking matrix, which is given as follows:

Table 11: Pugh Matrix for ranking Baselines

Characteristic	% WEIGHT	X45B	X45C	X47A	X47B
$C_{m'max\text{-}AC}$	0.05	2.35	2.95	5.00	2.28
$C_{d'max\text{-}AC}$	0.05	5.00	4.55	3.97	4.26
$C_{Lmax\text{-}AC}$	0.1	8.70	7.78	6.93	10.00
α_{Cli}	0.05	4.32	3.87	3.47	5.00
C_{di}	0.05	4.43	3.23	2.31	5.00
$C_{m'i}$	0.05	2.94	3.33	5.00	3.33
α_{CLmaxG}	0.05	4.34	3.87	3.44	5.00
$C_{d,ClmaxG}$	0.05	4.58	3.33	2.29	5.00
$C_{m'ClmaxG}$	0.05	2.94	3.30	5.00	3.30
RCS	0.5	40.93	49.31	50.00	44.98
Total	1	**80.53**	**85.52**	**87.40**	**88.15**

As evident, the best candidate has come out to be the Northrop Grumman X-47B, which is logical since it is the latest model out of all the aircraft that were analyzed. Therefore, our baseline design was selected as the Northrop Grumman X-47B.

CST Implementation in 3D

For parameterization, the planform of selected baseline i.e. X-47B was divided into four sections or breakpoints (BP), as shown in figure 34 at locations where leading edge or trailing edge sweep changed in a non-continuous manner. The wingtip was cropped for the sake of compatibility with AVL. Figure 35 shows parameterized model of X-47B using CST third order Bernstein Polynomial in both (chordwise and spanwise) directions. Here, the inverse CST uses Multi-objective Genetic Algorithm.

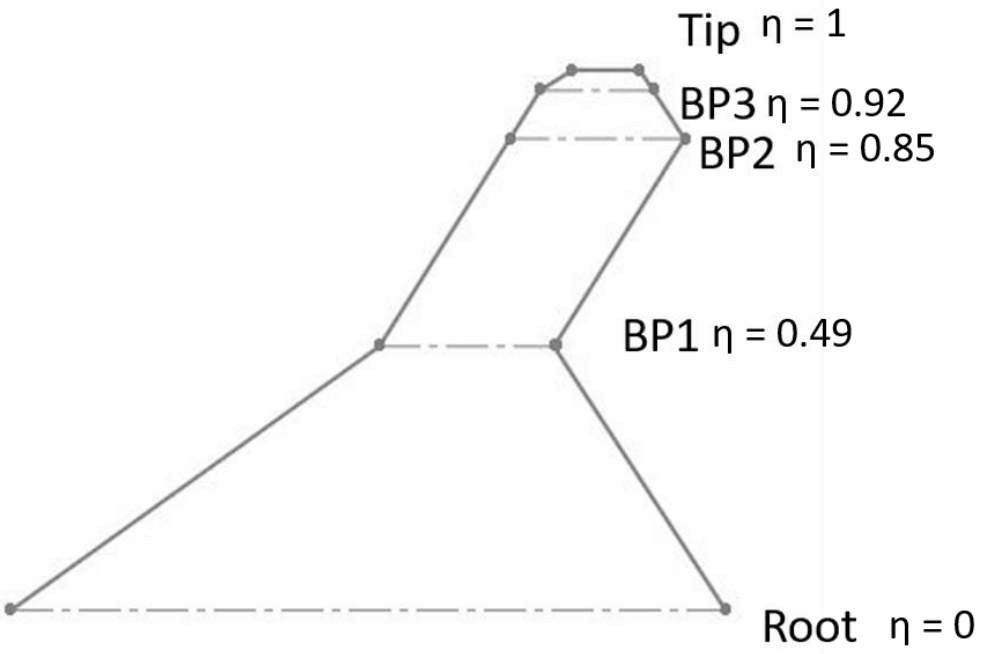

Figure 34: Planform divided into breakpoints

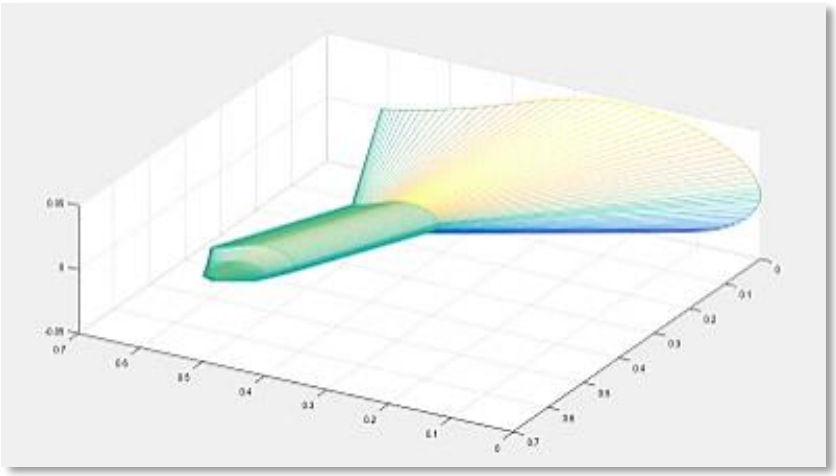

Figure 35: Parameterized Model of X-47B

Values of local chord and leading-edge x-coordinate which generated the xyz coordinates of wing profile shown in figure 33 are given in table 12

Table 12: CST Parameters for Wing

BP	η	x_{LE}	c_{LOC}
ROOT	0	0	0.61166
BP1	0.49	0.3401972	0.1407294
BP2	0.85	0.440899458	0.1368024
BP3	0.92	0.462607669	0.09282
TIP	1	0.51432038	0.02316454

To optimize wing planform, values of x_{le} and c_{loc} at BP1, BP2, BP3, and wing tip were chosen as variables. This made a total of 8 variables for optimization.

For Optimization Purpose, XFLR5 was not fit and a non-GUI software was needed which could also be coupled with MATLAB Computational Engine. Athena Vortex Lattice (AVL) served the job. A brief introduction of AVL is given below.

Athena Vortex Lattice (AVL)

AVL (Athena Vortex Lattice) 1.0 was originally written by Harold Youngren circa 1988 for the MIT Athena TODOR aero software collection (18). AVL is a program for the aerodynamic and flight-dynamic analysis of rigid aircraft of arbitrary configuration. It employs an extended vortex lattice model for the lifting surfaces, together with a slender-body model for fuselages and nacelles. General nonlinear flight states can be specified. The flight dynamic analysis combines a full linearization of the aerodynamic model about any flight state, together with specified mass properties (19).

AVL takes input in the form of wing defined in a file (.avl file). The wing definition is such that leading-edge location and local chord are defined at different spanwise sections. Some screenshots of its working are shown in figures 36 and 37.

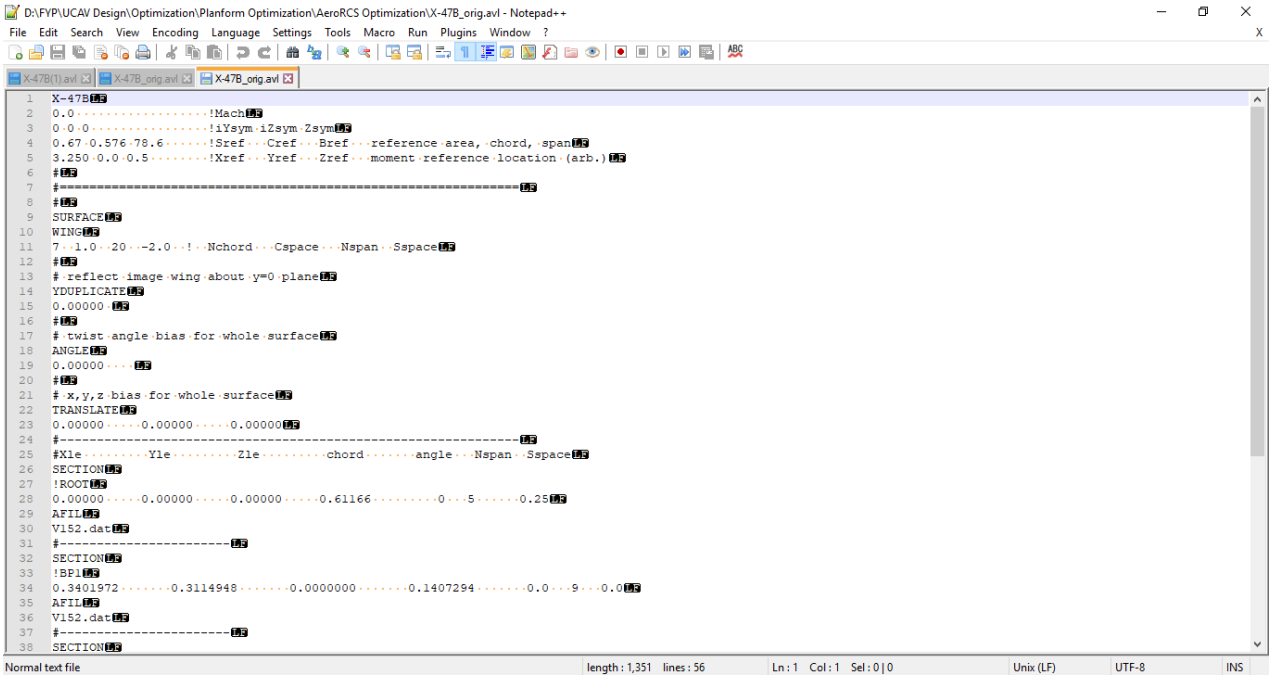

Figure 36: AVL Input File

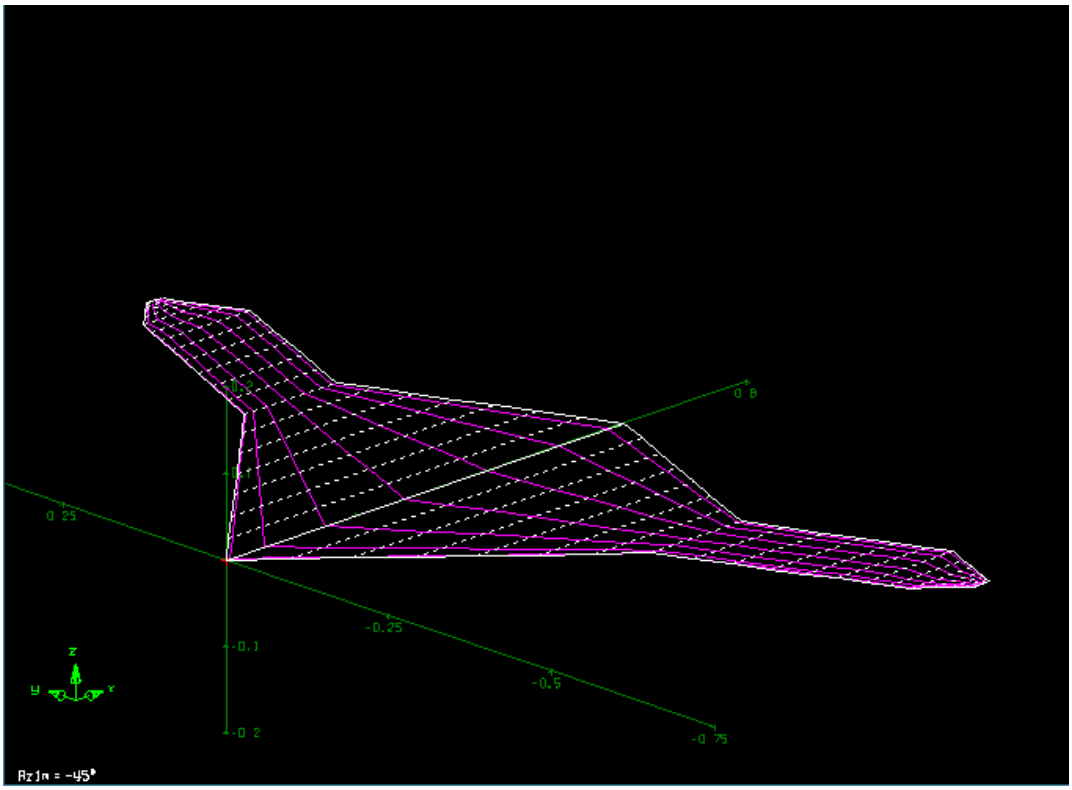

Figure 37: X-47B Baseline Geometry in AVL. Purple lines represent bound vortices of the Vortex Lattice (Screenshot taken from AVL)

Putting It All Together – Optimization Algorithm

After selecting and parameterizing X-47B as our Baseline planform, the final task was to make AVL, POFACETS, CST and MATLAB Optimization Toolbox work together on a single platform. For this, the following steps were taken.

- As mentioned earlier, we had eight variables in total so the design variables in vectorized form could be written as $\boldsymbol{[\vec{X}]} = (x_1, x_2, x_3, x_4, x_5, x_6, x_7, x_8) = (x_{le1}, x_{le2}, x_{le3}, x_{le4}, c_{loc1}, c_{loc2}, c_{loc3}, c_{loc4})$.
- These variables could be redirected to AVL via AVL-MATLAB interface (20). Lift to Drag Ratio (first objective function) could be extracted from there. The free stream velocity was set equal to cruise velocity i.e. 28 m/s. The lift coefficient required to lift the weight of aircraft at this speed was used by AVL to calculate design angle of attack, which turned out to be 7.16 degrees. All the aerodynamics calculations during optimization were preformed at this angle of attack.
- Bernstein Coefficients were still needed for airfoil definition but they were not design variables.
- Process of passing the design variables to POFACETS was more involved. First, these eight variables went through CST parameterization which converted them to xyz coordinates, so called Mesh (figure 35).
- Mesh triangulation was required to be done before redirecting it to POFACETS. This was accomplished using a program from MATLAB Central that converted a mesh (or surface) to stereolithographic (.stl) format (21) to create faceted geometry, as shown in figure 38. Note that stl file created from CST is coarser than the one shown in figure 28 which was created by SolidWorks. A decrement in accuracy ensues. Figure 39 shows a comparison of RCS patterns using the two types of faceted geometries.

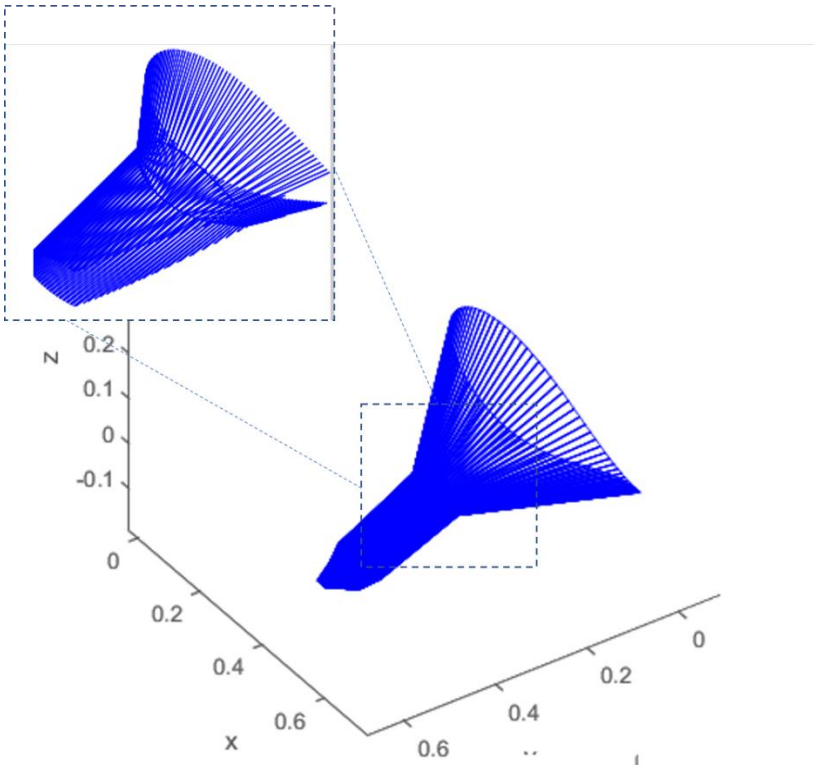

Figure 38: Mesh Triangulation

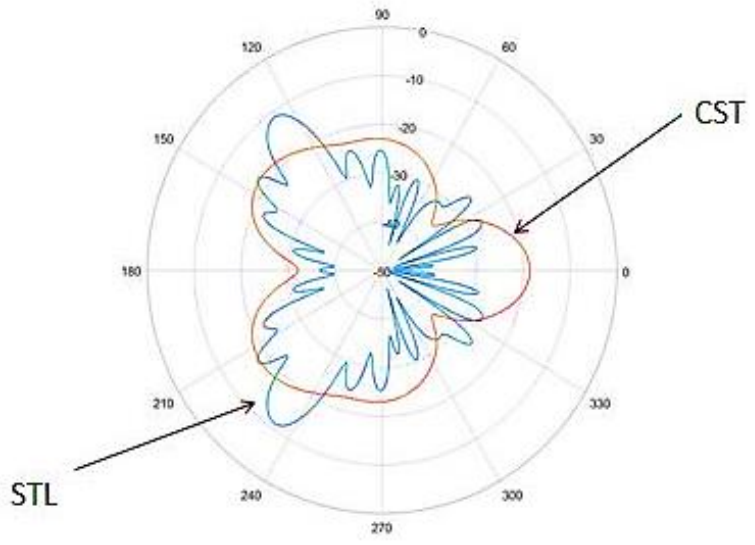

Figure 39: Comparison of accuracy of RCS Calculations from RCS Patterns

- The triangulated geometry is passed to non-GUI POFACETS for RCS calculation (second objective function).

- The upper and lower bounds of design variables are tabulated below.

Table 13: Lower and Upper Bounds of Design Variables

Lower Bound			Upper Bound		
Breakpoint	**xle**	**cloc**	**Breakpoint**	**xle**	**cloc**
BP1	0.206089	0.122332	**BP1**	0.42034268	0.366996
BP2	0.357593	0.073399	**BP2**	0.729349816	0.183498
BP3	0.390266	0.0367	**BP3**	0.79599041	0.100924
Tip	0.420125	0.000147	**Tip**	0.856890131	0.030277

This thinking process led us formulate the following algorithm for optimization.

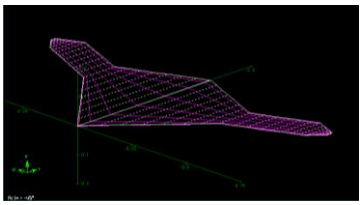

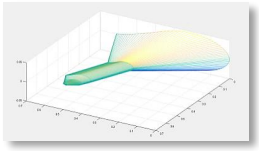

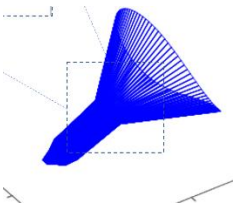

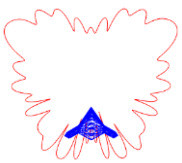

$B_{u\,ij}$, $B_{l\,ij}$
Initial values of c_{loc} and x_{le}
Initial Variables
GA
AVL MATLAB Interface
CST
L/D
Meshed Geometry
Triangulation
Non-GUI POFACETS
RCS
Convergence
Optimum Values of c_{loc} and x_{le}

CHAPTER 4: RESULTS AND DISCUSSIONS

Planform optimization

The optimization algorithm took 36 hours of computational time under default options of 'gamultiobj' command of MATLAB, resulting in a Pareto front (the fittest members) with 70 members. Results are shown in table 14. Figure 40 shows only 11 of them to avoid clutter.

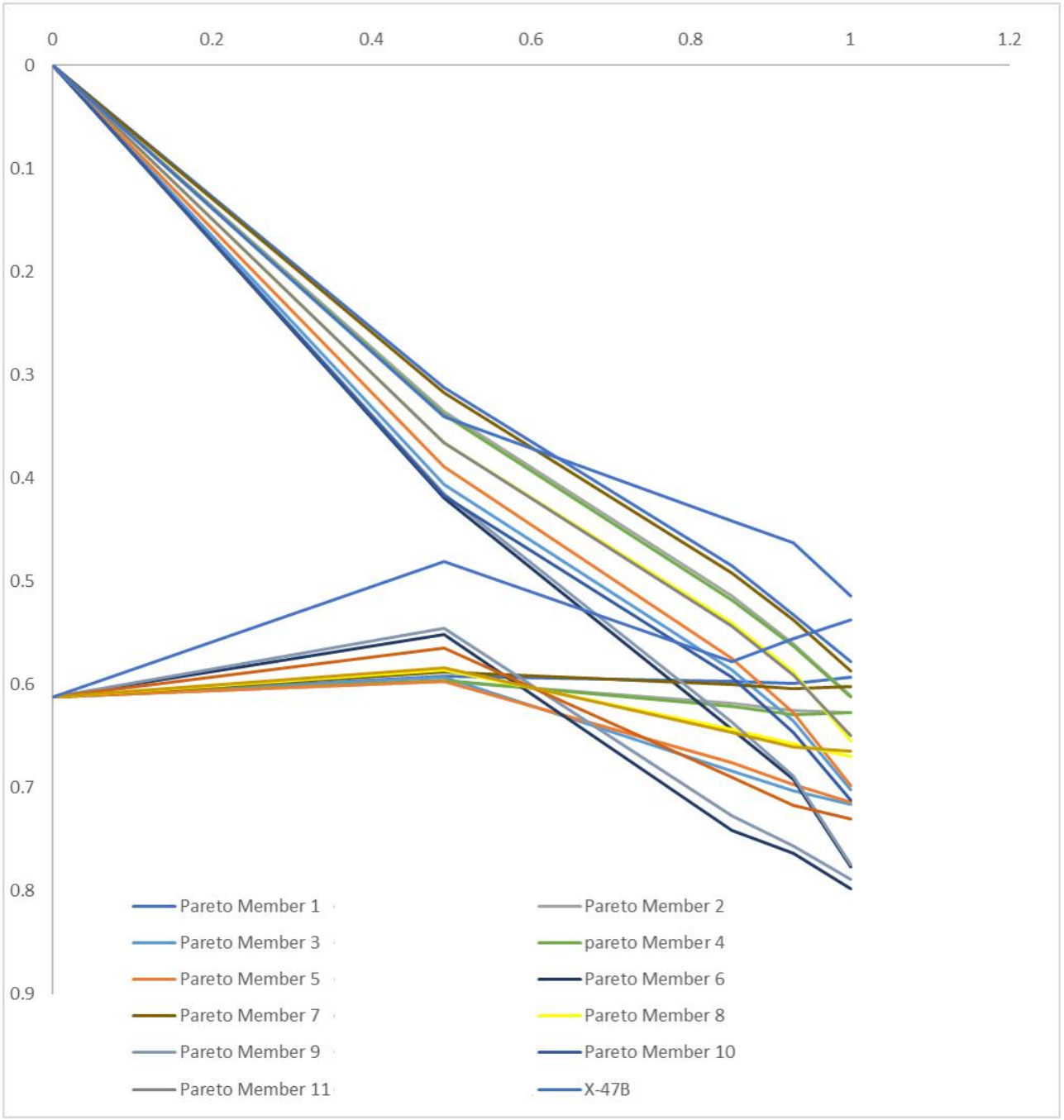

Figure 40: Pareto Front

Table 14: L/D and RCS of Pareto Members

Pareto Member	L/D	RCS (dBm^2)	Pareto Member	L/D	RCS (dBm^2)	Pareto Member	L/D	RCS (dBm^2)
1	26.65926	-48.9816	32	32.59222	-38.9717	63	27.56349	-47.3405
2	28.98683	-44.4212	33	32.77047	-38.4501	64	30.47607	-42.3935
3	27.56349	-47.3405	34	32.13472	-39.6865	65	27.03241	-48.5923
4	26.51188	-49.1386	35	27.33691	-47.6874	66	26.65926	-48.9816
5	28.88659	-44.6715	36	29.40883	-43.6533	67	28.7635	-44.9127
6	30.98346	-41.8749	37	34.42027	-35.6122	68	27.85903	-46.858
7	28.3093	-45.7425	38	30	-43.1585	69	32.41702	-39.2854
8	31.02043	-41.6718	39	29.25112	-43.6722	70	33.03293	-38.4322
9	27.67968	-46.9508	40	26.36866	-49.4864			
10	27.92355	-46.5699	41	33.2963	-37.6842			
11	29.73812	-43.2769	42	28.39916	-45.6416			
12	30.30435	-42.5597	43	31.77389	-40.4429			
13	30.11429	-42.7067	44	31.3199	-41.0326			
14	30.71696	-42.1892	45	33.20182	-37.8775			
15	30.47607	-42.3935	46	31.82249	-40.1908			
16	26.36866	-49.4864	47	34.03089	-36.9069			
17	32.68452	-38.7483	48	33.83119	-37.5243			
18	33.86943	-37.029	49	29.56078	-43.629			
19	33.19428	-38.1016	50	28.03597	-46.3337			
20	27.03241	-48.5923	51	33.59748	-37.6591			
21	30.82161	-41.9376	52	28.12435	-46.0785			
22	27.12668	-48.2689	53	29.1052	-44.2847			
23	34.44891	-35.2732	54	34.34448	-35.9123			
24	29.56128	-43.4077	55	34.23443	-36.2214			
25	29.18973	-43.8871	56	30.79449	-42.0579			
26	28.60897	-45.0118	57	32.21678	-39.36			
27	31.40707	-40.9264	58	34.44891	-35.2732			
28	33.84491	-37.4737	59	30.11456	-42.6908			
29	31.16795	-41.532	60	28.0587	-46.116			
30	28.44667	-45.3402	61	34.10749	-36.4387			
31	31.53104	-40.763	62	27.15511	-48.1255			

The criterion space as plotted by MATLAB is shown in figure 41.

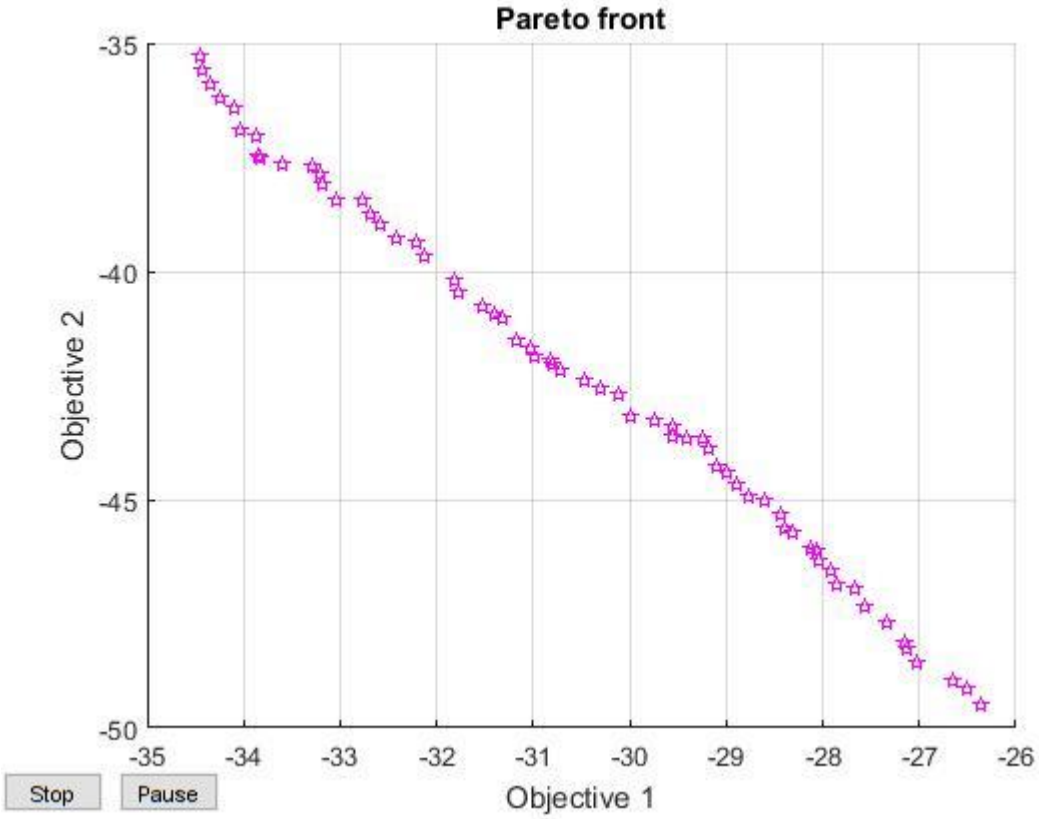

Figure 41: Criterion Space (The starred points represent Pareto Front). Objective 1 represents Lift to Drag Ratio (L/D) while Objective 2 is RCS

Note that L/D has negative values because optimization algorithm was built for minimization, by default.

From a physical interpretation point of view, the resulting pareto members seem optimized. This is supported by the fact that in some of them, wing aspect ratio has increased (increase in L/D) while in others, sweep angle has increased (decrease in RCS).

CHAPTER 5: CONCLUSION AND RECOMMENDATIONS

The project under discussion aimed to present a design of an Unmanned Combat Aerial Vehicle with maximized survivability, which is implied by a minimized Radar signature (RCS), and a maximized Aerodynamic performance (Lift-to-drag ratio), this was achieved by a multi-objective optimization using the Genetic Algorithm coded in MATLAB paired with AVL (for aerodynamic analysis) and POFACETS (for RCS analysis), the geometry for the aircraft was fed to the code in the form of Class-Shape Transformation (CST) parameters.

Some limitations of this work and possible refinements are:

1. Genetic Algorithm has different parameters (like maximum number of generations, maximum number of stall generations, cross over fraction, population size etc.) whose values need to be set before running the algorithm to get the best performance. Strictly Speaking, Pareto Front shown in figure 38 was obtained with default options/ parameters, already set in 'gamultiobj' command in MATLAB. However, one can use simple optimization techniques like Response Surface Method (22). The process is known as 'parameter tuning'.
2. Note that all of the pareto members are equally optimal unless a criterion for preference is specified as noted in (8), (23) and (24). Preferences can be specified before, during or after optimization process, which will yield a final optimized planform shape.
3. Panel Methods and Physical Optics for Aerodynamic and RCS Analyses respectively have their own limitations. For enhanced accuracy, one may couple Reynolds' Averaged Navier Stokes Equations with Maxwell's Equations in a high performance commercial software like ANSYS®.

Besides, there is a tremendous potential for further research in this work. Some of the recommendations are:

1. **Airfoil Optimization:** RCS of aircraft depends not only on planform shapes but also on the shape of airfoil, as noted in most stealth aircraft. One can optimize airfoil and planform simultaneously; interesting results will be observed. One such work was performed by Lee et al. (25)

2. **Aero-Stealth-Structural Optimization:** Stealthy airframes also have distinct design constraints. Structural integrity of such airframes can be ensured without compromising their aerodynamic and stealth performances.
3. **Aerodynamic and Stealth behavior in Swarm Flight**: The effect of swarming on Aerodynamic Performance and Low detectability can be explored and swarming formations can be optimized. These two design requirements can also be studied simultaneously with flight mechanics of swarming aircraft.

REFERENCES

1. Sadraey, Muhammad. *Aircraft Design, A Systems Engineering Approach.* s.l. : John Wiley and Sons, 2001.

2. Anderson, John D. *Fundamentals of Aerodynamics, 5th Edition.* s.l. : McGraw Hill Series in Aeronautical and Aerospace Engineering, 2011.

3. 3D VORTEX LATTICE METHOD. *Aerodynamics for Students.* [Online] http://www.aerodynamics4students.com/subsonic-aerofoil-and-wing-theory/3d-vortex-lattice-method.php.

4. Jenn, David C. *Radar and Laser Cross Section Engineering.* s.l. : AIAA Education Series, 2005.

5. Balanis, Constantine A. *Advanced Engineering Electromagnetics, Second Edition.* s.l. : John Wiley and Sons, 2012.

6. —. *Antenna Theory, Analysis and Design, 3rd Edition.* s.l. : John Wiley and Sons, 2005.

7. Sadiku, Matthew N. *Elementary Electromagnetics, 6th Edition.* 2014.

8. *Survey of Multi-Objective Optimization Methods for Engineering.* Marler, R. Timothy and Arora, Jasbir S. 2004.

9. Deb, Kalyanmoy. *Multi-Objective Optimization Using Evolutionary Algorithms.* Chichester, England : John Wiley & Sons, 2001.

10. Gudmundsson, Snorri. *General Aviation Aircraft Design, Applied Methods and Procedure.* s.l. : Elsevier Inc., 2014.

11. www.airfoiltools.com. [Online]

12. Jenn, David C. [Online] http://faculty.nps.edu/jenn/.

13. *A Universal Parametric Geometry Representation Method – "CST".* Kulfan, Brenda M. Reno, Nevada : AIAA, 2007.

14. *Parametric Airfoils and Wings.* Sobieczky, Helmut. s.l. : K. Fujii, G. S. Dulikravich (Ed.): Notes on Numerical Fluid Mechanics, Vol. 68, Vieweg Verlag.

15. MIT. XFOIL-Subsonic Airfoil Development System. *web.mit.edu.* [Online] https://web.mit.edu/drela/Public/web/xfoil/.

16. Palar, Pramudita Satria. How to fit your airfoil with CST parameterization? *WordPress.com.* [Online] https://pramsatriapalar.wordpress.com/2017/02/24/how-to-fit-your-airfoil-with-cst-parameters/.

17. Edelman, Louis. Xfoil Interface Updated. *MathWorks-File Exchange.* [Online] Mathworks. https://www.mathworks.com/matlabcentral/fileexchange/49706-xfoil-interface-updated.

18. Drela, Mark and Youngren, Harold. AVL Documentation. [Online] http://web.mit.edu/drela/Public/web/avl/.

19. MIT. AVL. [Online] http://web.mit.edu/drela/Public/web/avl/.

20. Moster, Joseph. *MathWorks-MATLAB Central.* [Online] https://www.mathworks.com/matlabcentral/fileexchange/45339-aerospace-design-toolbox.

21. McDonald, Bill. MathWorks File Exchange. *MATLAB Central.* [Online] https://www.mathworks.com/matlabcentral/fileexchange/4512-surf2stl.

22. *Using response surface design to determine the optimal parameters of genetic algorithm and a case study.* Kucukkocab, Ibrahim, Karaoglanb, Aslan D. and Yaman, Ramazan. s.l. : Taylor and Francis Group, 2013.

23. Arora, Jasbir S. *Introduction to Optimum Design, Second Edition.* s.l. : Elsevier Academic Press, 2004.

24. Arora, Rajesh K. *Optimization Algorithms and Applications.* s.l. : CRC Press, Taylor & Francis Group, 2015.

25. *Robust Evolutionary Algorithms for UAV/UCAV aerodynamic and RCS design optimisation.* Lee, D.S., et al. s.l. : Elsevier, 2008.